Cement and Concrete Research 161 (2022) 106946

Contents lists available at ScienceDirect

Cement and Concrete Research

journal homepage: www.elsevier.com/locate/cemconres

C-S-H seeding activation of Portland and Belite cements: An enlightening *in situ* synchrotron powder diffraction study

Alejandro Morales-Cantero [a], Ana Cuesta [a], Angeles G. De la Torre [a], Isabel Santacruz [a], Oliver Mazanec [b], Pere Borralleras [c], Kai Steffen Weldert [b], Daniela Gastaldi [d], Fulvio Canonico [d], Miguel A.G. Aranda [a,*]

[a] Departamento de Química Inorgánica, Cristalografía y Mineralogía, Universidad de Málaga, Málaga 29071, Spain
[b] Master Builders Solutions Deutschland GmbH, Albert-Frank Str. 32, 83308 Trostberg, Germany
[c] Master Builders Solutions España S.L.U., Carretera de l'Hospitalet, 147-149, Edificio Viena, 1ª planta, 08940 Cornellà de Llobregat, Spain
[d] Research & Development, Buzzi Unicem, Via Luigi Buzzi 6, 15033 Casale Monferrato, Italy

ARTICLE INFO

Keywords:
CO_2 footprint
Accelerators
C-S-H gel
Ettringite
Rietveld analysis
Synchrotron radiation

ABSTRACT

C-S-H seeding in Portland cements is well known from basic scientific works and field applications. Moreover, this activation approach could be beneficial for low-CO_2 cements under development where a general drawback is poor mechanical strengths during the first week of hydration. However, a mechanistic understanding of the different processes taking place when seeding is still not developed. Here, we contribute to this knowledge gap by studying one commercial Portland cement and two industrial-trial belite cements. Three different admixtures are employed, *viz.* two types of commercial C-S-H seeding and triisopropanolamine as a typical alkanolamine. A multitechnique approach is employed including calorimetry, ultrasonic pulse velocity, thermal analysis and Rietveld analysis of laboratory X-ray powder diffraction data. Chiefly, an *in situ* X-ray synchrotron diffraction study has allowed mapping out the evolution of every crystalline phase. Furthermore, the use of an internal standard permitted to measure the changes in the overall amorphous content. In a nutshell, alite and belite (phases) hydrations are not significantly accelerated by C-S-H seeding for the three studied cements. Conversely, sulphate and aluminate phase dissolutions are enhanced. Faster ettringite crystallisation contributes to the observed improved mechanical properties at early ages. Moreover, a synergistic effect between C-S-H seeding and alkanolamine addition is proved. The importance of these findings for the possible acceleration of low-CO_2 cement hydration is discussed.

1. Introduction

Portland cement (PC) industry has been in the last years strongly involved in improving its environmental performances. New cements with very low clinker contents are reaching market phase which currently seems the most efficient way to decrease the CO_2 footprint. Additionally, the use of alternative fuels has reached in some countries outstanding results with >90 % substitution of coal in some plants, and several projects dealing with Carbon Capture and Storage have started pilot phase. All these initiatives together are expected to attain carbon neutrality for cement sector in 2050. PC world production is currently ~4 Gt/yr, 4.1 Gt in 2019 [1], being the main component for the fabrication of mortars and concretes [2]. In turn, concrete is the most manufactured world commodity, ~5 t/person/yr. On average, every ton of grey Portland clinker generates ~0.87 tons of CO_2 [3] from limestone reaction and fuel consumption. The use of alternative fuels and improved process of production have shown the possibility to significantly reduce the amount of CO_2 released per ton of clinker but limestone decomposition is an unavoidable step. The environmental impact of PC production goes beyond CO_2 [4–6]. PC CO_2 footprint decrease was already recognized as a crucial requirement in the alleviation of the outcomes of climate change [4,7–9]. However, it is also known that to decarbonise cement production is very hard [10]. Producing infrastructures with longer service life [11,12] will contribute to CO_2 footprint reduction, as less cement will be needed in the future.

A principal work [8] named clinker replacement by supplementary cementitious materials (SCMs) [13,14] and concrete mixture proportioning [15] as the most advantageous ways for keeping the decrease of

* Corresponding author.
E-mail address: g_aranda@uma.es (M.A.G. Aranda).

https://doi.org/10.1016/j.cemconres.2022.106946
Received 5 November 2021; Received in revised form 28 June 2022; Accepted 11 August 2022

CO_2 footprint, now and in the near future. SCMs being currently the procedure with lowest impacts. However, other research approaches are needed to decrease cement CO_2 footprint for the medium future while always complying with current codes of practices. A way to make compatible the codes of practice with fabricating concretes with longer service lives and lower CO_2 footprints, allowing SCMs usage, is the use of cements where the main components are similar to those of PC, but with lower limestone demand: Belite cements (BCs). BCs have the same phases that PCs but the quantities of alite (C_3S) and belite (C_2S) are turned around (henceforth the cement terminology will be used). There are five advantages for BCs: (i) smaller temperature raise at early hydration times, and lower chemical shrinkage, which reduces thermal cracking; (ii) lower CO_2 direct emissions from limestone consumption, ~8 %; (iii) longer postulated service life, because the relatively larger content of C-S-H gel within the binder; (iv) lower kiln working temperature, ~1250–1300 °C, that may result in less additional gasses and easier kiln liner conservation; and (v) slightly less energy demand because the formation enthalpies for belite and alite are −2308 and −2931 kJ/mol, respectively [6]. However, there is one showstopper and three disadvantages for BC general usage. The showstopper is the slow reactivity of (non-activated) belite phase at ambient temperature yielding poor early-age strength developments. The disadvantages are: (i) they need ~15 % more grinding energy; (ii) the requirement of faster clinker cooling rates, which may end in larger energy demand and investment; and (iii) the limitation in using alternative fuels (due to the lower temperature required in the kiln for the clinker burning). Moreover, the combination of BC and SCMs is, so far, possible but less effective than PC. In this context, belite cements and their activations have been very recently reviewed [16].

As stated above, there is a clear need of increasing early age mechanical performances of BCs, mainly during the first week of hydration. This need is shared by several other low-CO_2 cements [17,18] like those based on high Portland clinker replacement by SCMs [4,13,14,19]. There are several approaches to accelerate early age cement hydration but not all are compatible with maintaining the long term strength as well as using highly available in the required quantities, not harmful, products which can be sustainable and cost effective. One approach could be seeding with water-based suspensions of C-S-H nanoparticles [20–22] and another the use of alkanolamines [23–26]. C-S-H seeding mainly accelerates C_3S hydration and alkanolamines the C_3A and C_4AF hydration. Furthermore, it is known that cement hydration is quite sensitive to alkanolamine dosage. In this context, a synergistic effect between C-S-H seeding and the addition of triethanolamine has been very recently reported [27].

The use of C-S-H nanoparticles in cement hydration has been reviewed [28,29] and it is not our intention to further review this topic here. Therefore, only some key aspects are developed next. C-S-H nanoparticle seeding has at least two main roles [28]. On the one hand, it provides additional (ideal) nucleation sites because the low interfacial energy, which may physically accelerate calcium silicate hydration, *i.e.* filler effect. On the other hand, the added nanoparticles can chemically influence the pore solution ion contents (*e.g.* Al^{3+}, SO_4^{2-}, Ca^{2+}, Na^{+}, K^{+}, *etc.*) as they can be adsorbed in the well-dispersed nanoseeds due to their high specific surfaces. In turn, the adsorption of selected ions from the pore solution may have two immediate consequences: i) the C-S-H growth mechanism(s) may be altered because the adsorbed species, and ii) the changes in the ions concentration in the pore solution, as well as C-S-H growth relatively far from the clinker surface, may create local concentration gradients which could alter the dissolution pathways in cementitious systems. These features add complexity as the hydrating systems may be further from equilibrium conditions. C-S-H seeding could be different in PCs, where there are many ions in the pore solution, when compared to pure alite samples, where pore solution is much more simple. Due to this, the present work does not elaborate on the role/consequences of C-S-H seeding in alite pastes. Here, it is only noted the complexity of the 'coupled dissolution/precipitation reactions' as previously deeply debated [30–32].

The current most accepted mechanism for explaining the consequences of C-S-H seeding is that the very early growth of C-S-H gel from alite dissolution is extended/accelerated by the new nucleation seeds within the capillary porosity. Synchrotron X-ray diffraction tomography has shown that C-S-H heterogeneous nucleation and growth process partly moves away from the dissolving clinker particles, enhancing secondary nucleation in the pore space of the hydrating paste [33]. The (partial) shift of the C-S-H gel from the surfaces of the C_3S to the pore space leads to a more homogeneous distribution of C-S-H products in the bulk of the paste [34], which in turn may reduce the mean pore volume, increasing the mechanical properties, and decreasing the water permeability of the resulting binder [35]. However, it is acknowledged that C-S-H nanoparticles prepared under different conditions, and hence having different properties, could result in a range of final performances after cement activation [36]. Furthermore, it has also been reported the influence of PC mineralogy [37] and cement fineness, as for cements with larger surface area, acceleration is lowered when adding the same amount of the same seeds [37]. Several other parameters may also intervene like the sulphate and alkaline ion contents or the hydrating temperatures [38].

Next, it is discussed the main techniques which are being currently used to characterise C-S-H seeding for PCs [28,29] and also for low-CO_2 cements: both BCs [39] and those obtained by replacement of PC clinker by SCMs [27,34,40–45]. By far, the most employed techniques are calorimetry and mechanical strength measurements. This is expected as mechanical strength characterisation at different hydration ages yield a picture of the performances of the resulting binders and calorimetry is widely-available and it allows systematically comparing the heat flow of designed series by measuring the ends of the induction period and the maximum heat developed at early ages, which are the most prominent features of cement hydration acceleration. Mercury intrusion porosimetry and scanning electron microscopy have also been employed to characterise the porosities and C-S-H distribution and chemical characteristics, respectively. Furthermore, thermal analysis yields additional valuable information like the total chemically bound water and the amount of portlandite. From all these characterisation tools, only portlandite content from thermal analysis gives phase-related information but it must be considered that it can be consumed by pozzolanic reaction, the formation of AFm phases and even by carbonation, if the experimental conditions are not fully controlled. However, and to the best of our knowledge, Rietveld quantitative phase analysis of powder diffraction data for seeded Portland cements has not been employed to accurately determine the degree of reaction of the main crystalline components of the pastes. It is needless to say that to optimise cement hydration, it is important to measure the degree of hydration of all components of the cements. This work addresses this knowledge gap.

Here, three activation procedures have been studied (two types of C-S-H seed systems and triisopropanolamine, TIPA) in three industrially-produced cements (a typical 42.5 PC and two BCs). Initially, the calorimetric and the mechanical strength studies characterise the cement hydration activations, as viewed from these two overall complementary perspectives. Secondly, laboratory characterisation (thermal analysis and *ex situ* Rietveld analysis of laboratory powder diffraction data) at 2, 7 and 28 hydration days is carried out to contribute to the understanding of the activation mechanism(s) by determining the degree of reactions of the main crystalline phases. Finally, Rietveld analysis of *in situ* synchrotron powder diffraction data at very early ages, <48 h, allowed to quantitatively determine the phase content evolutions with time and with the activators. It is shown that sulphate and aluminate dissolutions and ettringite crystallisation, and not alite hydration, are the main mechanisms for early age cement activation.

2. Materials and methods

2.1. Starting material provenance

Three cements have been used in this study: a commercial Portland cement, CEM I 42.5 R, **PC-42.5**, which conforms to EN 197–1; a Belite cement, CEM I 42.5 N-like, provided by Buzzi Unicem SpA (Italy) [46], **BC-Buz**, which was activated by sulphur during the clinkering stage; and a non-activated Belite cement, **BC-n.a.** The latter was prepared as follows: 10 kg of nodules of belite clinker were crushed up to <2 mm particles. The crushed clinker was milled in batches of 1.2 kg in a ball mill at 50 rpm from Proeti S.A., with 9 kg of steel balls of 9, 18 and 32 mm of diameter, during 8–10 h until desired Blaine, by stopping each hour to avoid overheating. A natural gypsum rock sample was milled in the same ball mill for 1 h. The BC-n.a. was prepared by homogenizing 95 wt% of BC clinker and 5 wt% of milled gypsum in a micro-Deval machine at 100 rpm during 12 h, with 8 steel balls of 24 mm diameter. The characterisation of the employed gypsum is given in the Supplementary Information (S.I.).

Quartz, SiO_2, 99.5 %, Alfa Aesar, was used as internal standard in the *in-situ* SXRPD study to indirectly determine the overall amount of amorphous and unidentified components (ACn) of the pastes [47]. All the anhydrous cements were manually mixed in an agate mortar with ~12 wt% of Quartz. Three commercially available admixtures, acting as accelerators of hydration, have been used: triisopropanolamine (98 %, Acros Organics), and C-S-H gel-based seeds: Master X-Seed 100 (XS100) and Master X-Seed 130 (XS130) both from Master Builders Solutions España S.L.U., Spain. Master X-Seed 100 is a concentrated suspension of C-S-H nanoparticles in water, with a solid content ranging 20–22 %. Meanwhile Master X-Seed 130 has a solid content ranging 28–30 % and it also incorporates alkanolamines.

2.2. Pastes and mortars preparation

Pastes were prepared with a constant w/c (water-to-cement) mass constant ratio of 0.50. For the *in situ* synchrotron diffraction study and the isothermal calorimetry the paste preparation was carried out by, first, magnetically stirring of the water with the admixture during 1 min, then mixing the cements with the dissolution/diluted suspension and shaking during 1 min manually and then during 1 min with a vortex mixer. Then, the samples were injected with a syringe in the borosilicate capillaries of 0.7 mm of diameter for *in situ* synchrotron study or inserted into the glass ampoules and then in the calorimeter for the isothermal calorimetry measurements.

The amounts of admixtures added were 2 wt% (of the as received product) for XS100 and XS130, and 0.05 wt% (of active matter) for TIPA; always by weight of cement. In the case of XS100 and XS130, the added water was recalculated taking into account the water content of the admixtures in order to maintain the w/c ratio of the pastes fixed, *i.e.* 0.50. These dosages are typical of field applications in PC-based concretes.

For the *ex situ* diffraction study, the pastes were stirred at 800 rpm for 90 s, then a pause of 30 s and another stirring step (800 rpm/90 s). Subsequently, the pastes were casted within cylinders (10 mm of diameter and 35 mm long) and maintained for 24 h. After demoulding, the specimens were kept in water until needed. To minimise calcium leaching, the cylinders where packed within a tightly closed bottle with the smallest-possible amount of water. To stop the hydration, the pastes were grinded, filtrated, washed with isopropanol twice and then with diethyl ether.

Mortars with water/cement/sand mass proportions of 0.50/1/3 were mixed following EN196-1 and casted into 40 × 40 × 160 mm^3 moulds. Specimens were de-aired by knocking 60 times the half-casted moulds, then fully filled and another 60 knocks were carried out in a jolting table UTCM-0012, 3R (Montauban, France). The samples were kept in the moulds (20 °C and 99 % RH) for 24 h. Then, the prisms were demoulded and placed within water, $T = 20$ °C, for the required periods of time.

2.3. Analytical techniques

2.3.1. Textural characterisation

Specific surface areas were determined by N_2 isotherms in a ASAP 2420 (Micromeritics, USA) device. Blaine fineness apparatus (Controls) was employed to get the air permeabilities following EN 196–6. Particle size distribution (PSD) data were acquired in a MasterSizerS equipment (Malvern) with powder suspensions in ethanol.

2.3.2. X-ray fluorescence analysis

For PC-42.5, the analysis was carried out with a PANalytical Axios max equipment (Financiera y Minera S.A.). For BC-Buz and BC-n.a., the measurements were done with an ARL ADVANT'XP+ Thermo Fisher device (SCAI– Universidad de Málaga).

2.3.3. Transmission Electron Microscopy (TEM) study

The morphology and size of the C-S-H seeds of the employed accelerators (XS100 and XS130) were characterised by TEM. A JEM-1400 (Jeol, Japan) microscope, equipped with a Gatan ES1000W camera, was used working at 80 kV. The commercial suspensions were diluted (1/1000) with isopropanol and introduced in an ultrasound bath for 10 s. Subsequently, they were deposited on Cu grids, 200 mesh, with formvar-carbon films.

2.3.4. Isothermal calorimetry

An eight channels Thermal Activity Monitor (TAM) instrument with glass ampoules was used. The paste preparation has been detailed in Subsection 2.2. The heat flow curves were collected up to 7 days at 20 °C. The first 45 min after mixing are not collected to ensure stabilisation of the equipment.

2.3.5. Ultrasonic pulse measurement study

The ultrasonic pulse velocities (UPV) through the studied mortars, prepared as described just above, were monitored by an IP8 ultrasound system (UltraTest GmbH) during the first four days of hydration. The device is located within a laboratory with a constant temperature of 19 ± 1 °C. The variation of the velocities reflects the setting and microstructural development of the mortars as low velocities are measured for flowable mortars, meanwhile high velocities are acquired for hardened binders where connectivities between solid phases are being developed. Pastes were not measured as bleeding was observed during the first hours likely as consequence of the ultrasonic waves. Two key advantages of this method are: i) it yields *continuous in-situ* data related to the microstructural developments without sample treatment; and ii) it needs low amount of sample, in this case ~80 g of the cements. The frequency of the ultrasonic wave was 30 kHz and the distance between the receiver and the transmitter was 40 mm. The temperature of the mortars was also continuously monitored.

2.3.6. Compressive and flexural strengths

Mechanical data for mortars were determined following EN196-1. The employed press was Autotest 200/10 W (Ibertest, Madrid, Spain) working at 1.5 $MPa \cdot s^{-1}$ rate. The measurements were done at 1, 7 and 28 days of hydration. Flexural data were taken in three prisms. Compressive data were taking in the six resulting specimens. The reported data are the averages of all corresponding measurements.

2.3.7. Rheological behaviour

The effect of the admixture on the rheological behaviour of BC-Buz mortars was studied. A rheometer (Model VTiQ AIR, Thermo Scientific Haake, Karlsruhe, Germany) with a VANE rotor system (FL16 4B/SS, with 16 mm of diameter) in a serrated cup (CCB43-C48/SE) was used. The gap between the end of the blade and the inner cup was 13.175 mm. Mortars were pre-sheared at 160 rpm during 0.5 min, and after that,

controlled rate measurements were recorded from 150 rpm to 5 rpm, every 5 rpm, with stabilisation times of 10 s at every step.

2.3.8. Thermal analysis (TA)

Thermogravimetric data (TGA), for the hydration-stopped pastes, were recorded in a SDT-Q600 analyser from TA instruments (New Castle, DE). Temperature was increased, 10 °C/min rate, from RT to 40 °C, then kept at this temperature for 30 min and finally elevated up to 1000 °C. Samples were placed in open Pt crucibles with synthetic air flow. The weighed loss from 40° to 550 °C was assigned as bounded water and the mass loss in the 550–1000 °C range was taken as CO_2. The free water (from TGA data: FW_{TA}) in wt%, was determined from the losses in the 40–550 °C range, knowing the amount of added water, using Eqs. (4) and (5):

$$BW = \frac{BW_{TA} \times CM}{100 - BW_{TA}} \quad (4)$$

$$FW_{TA} = TW - BW \quad (5)$$

where BW is the chemically bounded water amount, TW is the total water content (in this case 33.3 wt%), BW_{TA} is the weight loss in the 40–550 °C temperature range from TA data, of the pastes after stopping the hydration, and CM is the cement content.

2.3.9. Ex situ laboratory X-ray powder diffraction (LXRPD)

A D8 ADVANCE (Bruker AXS) powder diffractometer (SCAI–Universidad de Málaga), which worked in θ/θ geometry with Mo-Kα_1 radiation, λ = 0.7093 Å, was used to collect the patterns for all the anhydrous cements and the arrested pastes after 2, 7 and 28 days. The powdered samples were prepared manually between two Kapton foils without pressing. Rietveld analyses were performed using the GSAS suite of programs and the EXPGUI graphic interface [48]. The hydration stopped pastes were blended with quartz as internal standard, approximately 20 wt%, to derive the ACn amount [47].

2.3.10. In situ synchrotron X-ray powder diffraction (SXRPD)

The *in situ* SXRPD study was performed in the powder diffraction end station of the MSPD-BL04 beamline at ALBA synchrotron (Barcelona, Spain) [49]. The selected wavelength was 0.62005(1) Å (20 keV). The detector used was MYTHEN which is especially suited for time-resolved experiments and provides a good signal-to noise ratio with short acquisition times. The data collection time was 6 min per pattern in the angular range from 2 to 40° (2θ). The four capillaries sample holder was used and rotated at 20 rpm during measurement for better powder averaging. The period of ~3 to ~19 h was continuously measured for PC-42.5 and BC-Buz pastes, while up to ~37 h for the BC-n.a. ones (longer overall data collection to use the last night of the synchrotron experiment).

The SXRPD patterns were analysed by using the Rietveld methodology with GSAS-II software [50]. The instrumental parameters were determined from the pattern of Si SRM 640e standard collected in exactly the same conditions: U = 16.96, V = −2.50, W = 0.75, X = 0.17, Y = 1.34, Z = 0.0 (0.01°) and SH/SL = 0.002. The crystal structures used are those published elsewhere [51,52]. The ACn values have been determined by the internal standard methodology [47]. This value includes the decreasing free water (FW) fraction, the increasing C-S-H gel content and any other amorphous components (for instance any ill-crystallised hydrated phase like iron-siliceous hydrogarnet).

2.3.11. Calculated phase and water contents based on chemical reactions

A post-analysis calculation was performed to estimate the amount of free water and the amount of amorphous C-S-H gel [53] from the hydration reactions for different phases under certain assumptions. Details about these calculations are given in S.I.

3. Results and discussion

3.1. Characterisation of the starting materials

The three cements have been analysed by XRF, SXRPD and LXRPD. The full characterisation of the three cements is deposited as S.I. Table S1 gives the elemental compositions from XRF. Tables S2 and S3 give the mineralogical compositions from SXRPD and LXRPD, respectively. A minor variability is observed which is in line with different experimental procedures and the sampling effects. Fig. S1 displays the three SXRPD Rietveld plots which are the basis for the reported RQPA results, t_0, given in Tables 1–3. The textural properties are also key to understand the early age reactivities. Thus, a full textural analysis was carried out. The Blaine results were 370, 502 and 429 m^2kg^{-1} for PC-42.5, BC-Buz and BC-n.a., respectively. The related BET surface areas, in the same order, were 1.20(1), 1.40(1) and 1.20(1) m^2g^{-1}. The PSD traces are displayed in Fig. S2 with $d_{v,50}$ being 18.1, 12.8 and 8.0 μm for PC-42.5, BC-Buz and BC-n.a., respectively. BC-Buz was employed in two previous studies [54,55] but its full characterisation is reported here for the sake of completeness.

A detailed characterisation of the admixture can be found in the original patent [56] including the particle size distribution, Fig. 2 of that document. In any case, the particle sizes and morphologies of the employed seeds have been studied by TEM as variability in commercial products is to be expected. Fig. 1 displays relatively large views of the dispersed C-S-H seeds showing variable particles sizes ranging from about 50 nm to 200 nm. Enlarged views, one agglomerated particle for each admixture, are also displayed to highlight the foil-like nature of these amorphous solids. Similar particles sizes and morphologies have been very recently reported for XS100 [38] and XS130 [57].

3.2. In situ calorimetric study of pastes

Fig. 2 displays the calorimetric study for all the studied samples showing the effects of the employed accelerators as seen in the cumulative heat traces. Fig. 3 shows the heat flows for the cements with the studied admixtures. As expected, the hydration of PC is accelerated at early ages by the XS100 and XS130 admixtures [37]. The end of the induction period shortens from 2.6 to about 2.0 h, see Fig. 3a. Here it is followed the standard approach dividing the calorimetries in three periods: i) up to the end of the induction, ii) main heat evolution peak, and iii) continuing reactions at later ages [58,59]. The height of the first peak, which is mainly due to the hydration of alite is also increased and narrowed, see Fig. 3a. Quantitative data from the calorimetries are given in Table S4 including the end of the induction period (IP) determined by the interception of two straight lines as depicted in Fig. 3a. It can be observed that TIPA, at the dosage used in this study, does not modify the IP, but it increases the overall heat released at 7 days, see Fig. 2a.

BCs liberate lower hydration heat, when compared to PCs, because the slower hydration kinetics and also because the hydration of belite develops less heat than that of alite [16], see Fig. 2c. It can be seen that BC-Buz is not significantly accelerated at very early ages, <12 h, by XS100 neither TIPA, see Fig. 3c. Conversely, XS130 accelerates the very early hydration as the heat flow peak at ~11 h increases notably. It should also be noted that the shape of the first peak is modified, narrowed, by this admixture. In addition, TIPA increases the heat flow development after the first peak at ~20 h. The chemical reactions associated to these processes will be discussed in the *in situ* synchrotron powder diffraction subsection. Concerning the total heat flows released at 7 days, XS100 does not significantly modify the reference value. However, the pastes containing XS130 and TIPA released more heat, ~10 %, at this hydration age, see Table S4 and Fig. 2c.

The calorimetries for BC-n.a. are given in Figs. 2e and 3e. Like for PC and BC-Buz, TIPA does not significantly affect the IP of this cement. However, after five days the paste containing this admixture released more heat, see Table S4. As shown in Fig. 3e, XS100 accelerates the

Table 1
RQPA results for PC-42.5 pastes with ACn determined by the internal standard method and FW determined by TA. In italics, theoretically calculated values. These pastes at t_0 also contain: 0.7 wt% of $C\bar{S}H_2$ and 1.3 wt% of $C\bar{S}H_{0.5}$.

Phases	t_0	PC-42.5-Ref			PC-42.5-XS130			PC-42.5-TIPA		
		2d	7d	28d	2d	7d	28d	2d	7d	28d
C_3S	33.3	12.8	8.3	4.2	13.0	8.3	3.7	13.5	8.5	3.7
DoR[a]/%		*62*	*75*	*87*	*61*	*75*	*89*	*59*	*74*	*89*
C_2S	5.0	6.6	5.2	5.3	7.2	6.9	6.3	7.4	7.9	7.0
DoR[a]/%		–	–	–	–	–	–	–	–	–
C_4AF	6.4	6.7	4.7	3.2	6.2	4.1	2.5	6.9	5.9	4.5
DoR[a]/%		–	*27*	*50*	*3*	*36*	*61*	–	*8*	*30*
C_3A	4.5	2.8	1.6	0.9	2.2	1.4	0.8	2.9	1.6	0.9
DoR[a]/%		*38*	*65*	*80*	*51*	*69*	*82*	*36*	*65*	*80*
$C\bar{C}$	2.4	5.1	2.8	1.8	5.2	4.3	2.1	5.1	5.0	2.3
CH	–	7.8	10.0	12.0	6.6	8.7	11.2	7.2	9.8	11.6
AFt	–	6.0	8.1	7.7	7.1	8.5	8.1	5.8	7.2	6.5
AFm-Hc	–	–	–	–	–	0.8	0.8	–	–	0.6
AFm-Mc	–	–	–	0.8	–	–	1.0	–	–	1.3
ACn	13.0	29.0	37.8	46.0	29.9	37.6	46.2	27.4	34.4	44.2
FW_{TA}[b]	33.3	23.3	21.4	18.1	22.6	19.4	17.3	23.7	19.7	17.6
C-S-H	–	*20.7*	*25.9*	*30.6*	*19.0*	*24.2*	*29.8*	*19.6*	*25.5*	*30.3*
Other ACn	*13.0*	*9.2*	*14.8*	*17.9*	*11.2*	*14.2*	*18.3*	*8.5*	*9.5*	*15.4*
FW[c]	33.3	*22.4*	*18.5*	*15.6*	*22.3*	*18.6*	*15.4*	*23.0*	*19.1*	*16.1*

[a] DoR stands for degree of reaction/hydration respect to t_0.
[b] FW_{TA} (free water) content determined from thermal data as described in the experimental section.
[c] FW (free water) content calculated from the assumed chemical reactions as described in S.I.

Table 2
RQPA results for BC-Buz pastes with the format given in Table 1. These pastes at t_0 also contain: 1.4 wt% of $C\bar{S}$.

Phases	t_0	BC-Buz-Ref			BC-Buz-XS130			BC-Buz-TIPA		
		2d	7d	28d	2d	7d	28d	2d	7d	28d
C_3S	15.3	4.8	4.2	3.5	6.1	4.2	2.8	5.4	3.0	2.2
DoR/%		*69*	*72*	*77*	*60*	*72*	*82*	*65*	*80*	*86*
C_2S	31.3	29.5	28.0	18.6	29.5	23.8	16.0	30.3	28.2	22.9
DoR/%		*6*	*11*	*41*	*6*	*24*	*49*	*3*	*10*	*27*
C_4AF	6.9	4.9	4.0	1.7	2.9	1.7	1.1	4.1	3.1	1.7
DoR/%		*29*	*42*	*75*	*58*	*75*	*84*	*40*	*55*	*75*
C_3A	*2.3*	–	–	–	–	–	–	–	–	–
$C_4A_3\bar{S}$	1.2	0.5	–	–	0.4	–	–	0.4	–	–
$C\bar{C}$	2.3	5.5	0.9	1.2	4.1	1.3	0.9	4.6	4.1	0.7
MgO	1.2	1.0	0.9	0.8	0.9	0.9	0.9	1.0	0.9	0.9
CH	–	2.9	3.5	4.0	2.3	2.9	3.5	2.5	3.1	3.8
AFt	–	9.4	8.9	13.1	10.2	12.9	12.5	9.0	10.7	10.0
AFm-Hc	–	–	0.3	0.5	0.8	1.9	1.4	0.4	1.0	1.3
AFm-Mc	–	–	–	1.0	–	–	–	–	–	2.6
Katoite	–	–	0.5	0.8	–	0.5	0.5	–	0.5	0.6
ACn	4.8	17.3	26.7	34.7	19.9	28.8	42.4	18.7	23.0	34.8
FW_{TA}	33.3	24.2	22.1	20.1	22.9	21.0	18.0	23.6	22.4	18.5
C-S-H	–	*9.2*	*11.8*	*19.1*	*7.6*	*13.8*	*20.6*	*8.3*	*11.6*	*16.6*
Other ACn	*4.8*	*7.2*	*13.3*	*15.9*	*10.4*	*14.6*	*20.7*	*8.7*	*10.7*	*16.1*
FW	*33.3*	*25.1*	*23.7*	*19.8*	*24.8*	*21.4*	*19.1*	*25.3*	*23.1*	*20.6*

hydration of this cement as the IP shortens from ~10 to ~7 h. However, the total heat released by the paste containing this admixture at 7 days is nearly the same than that of the reference paste, see Fig. 2e. On the contrary, XS130 accelerates the very early hydration, see Fig. 3e, and it also notably increases, ~15 %, the total heat liberated at 7 days, see Table S4. Furthermore, this admixture, and for this cement, strongly affects the ettringite crystallisation as a very narrow, and intense, peak is detected at 15 h. This is also detected in the UPV study, see next, and it will be explained in the *in situ* synchrotron powder diffraction subsection.

3.3. In situ ultrasonic test measurements of mortars

To better understand the effects of the accelerating admixtures on the cement hydration processes, including the microstructural development of the mortars, an ultrasonic measurement study has been carried out. The results of this investigation are displayed in the right panels of Figs. 2 and 3. Fig. 2b, d and f displays the typical S-shaped curves which are commonly discussed in three main stages [60,61]. The first stage is the induction period and it lasts ~1–2 h for mortars. The low velocities of the ultrasonic pulses when travelling through the viscous suspension are due to the strong reflections and attenuation from the air entrapped in the mixtures. Hence, the observations from this period are not discussed in this investigation. The second stage is characterised by a fast increase in the velocities which is due to the formation of new hydrated products connecting the solid particles. Here, the mixture evolves from a liquid suspension to a solid network. In the third stage, the velocities increase much more slowly and they eventually get constant yielding values close to 4100–4500 m/s for neat PC-mortars. Depending upon the binder, somewhat larger increase in velocities can be observed during this third period, ~2–7 days, due to additional filling of capillary pores with products formed by slow-rate reactions, for instance for blends with SCMs [62].

Fig. 2b displays the UPV traces for the four mortars based on PC-

Table 3
RQPA results for BC-n.a. pastes with the format given in Table 1.

Phases	t_0	BC-n.a.-Ref			BC-n.a.-XS130			BC-n.a.-TIPA		
		2d	7d	28d	2d	7d	28d	2d	7d	28d
C_3S	19.4	3.7	2.4	1.7	4.7	2.3	1.2	4.7	2.0	1.6
DoR/%		*81*	*88*	*91*	*76*	*88*	*94*	*76*	*90*	*92*
C_2S	31.6	31.5	34.5	24.9	32.6	33.7	17.9	35.9	33.8	27.2
DoR/%		–	–	*21*	–	–	*43*	–	–	*14*
C_4AF	9.6	7.5	6.4	6.7	6.3	5.3	2.9	8.9	6.3	3.6
DoR/%		*22*	*33*	*30*	*34*	*45*	*70*	*7*	*34*	*63*
$C\overline{S}H_2$	1.9	0.4	0.3	0.4	0.5	0.3	0.5	0.6	0.7	0.9
$C\overline{C}$	–	3.1	–	–	2.4	–	–	1.0	0.9	–
CH	–	4.4	5.0	4.9	3.3	4.2	5.1	4.5	4.5	4.3
AFt	–	4.9	5.2	3.0	4.7	4.8	4.3	4.5	5.2	3.6
AFm-Hc	–	–	0.3	0.4	–	0.4	0.6	–	–	–
ACn	4.2	17.9	21.6	37.6	19.3	24.9	47.6	14.0	21.1	37.2
FW_{TA}	33.3	26.6	24.3	20.4	26.2	24.1	19.9	25.9	25.5	21.6
C-S-H	–	*13.8*	*15.2*	*20.0*	*11.8*	*14.2*	*25.2*	*13.0*	*14.8*	*17.7*
Other ACn	*4.2*	*4.3*	*5.2*	*15.3*	*6.7*	*9.1*	*22.5*	–	*6.1*	*18.1*
FW	*33.3*	*26.4*	*25.5*	*22.7*	*27.0*	*25.7*	*19.8*	*26.9*	*25.7*	*23.0*

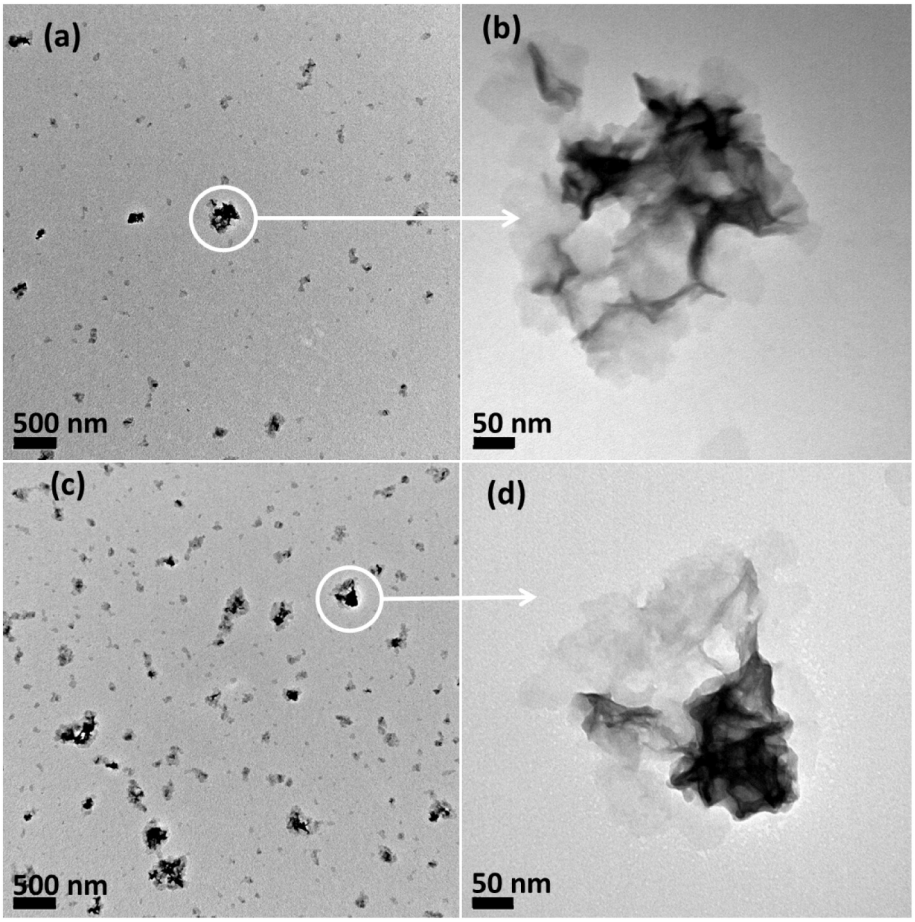

Fig. 1. TEM images for the employed C–S–H seeds. (a) 25,000× selected view of XS100 admixture dispersed in isopropanol; (b) zoom magnification, 250,000×, showing an agglomerated foil-like cluster; (c) 25,000× view of XS130; and (d) zoom magnification, 250,000×, showing an agglomerated foil-like cluster.

42.5R. During the second stage, the traces for PC-42.5-Ref and PC-42.5-TIPA are nearly the same. In the third period, TIPA led to higher velocities which implies more connected particles. Importantly, at early ages the velocities for PC-42.5-XS100 and PC-42.5-XS130 increases at higher rates which is a clear signature of hydration acceleration. This is better observed in the derivative traces, also known as acceleration curves, displayed in Fig. 3b. The maxima of the acceleration curves for the reference and TIPA mortars take place at ~4 h. However, XS100 and XS130 displaced these values to 3.0 and 2.8 h, respectively. We justify that the maxima of the acceleration process as measured by UPV in mortars, 3–4 h, take place earlier than those measured by calorimetry in pastes, 8–11 h, see Fig. 3a, because the larger amount of surfaces provided by the sand and because the higher (shear) energy during mixing of the mortars. Moreover, the aluminate peaks also take place earlier in mortars (as detected by UPV) than in pastes (as detected by calorimetry). For instance, the enhanced aluminate peak for PC-42.5-TIPA takes

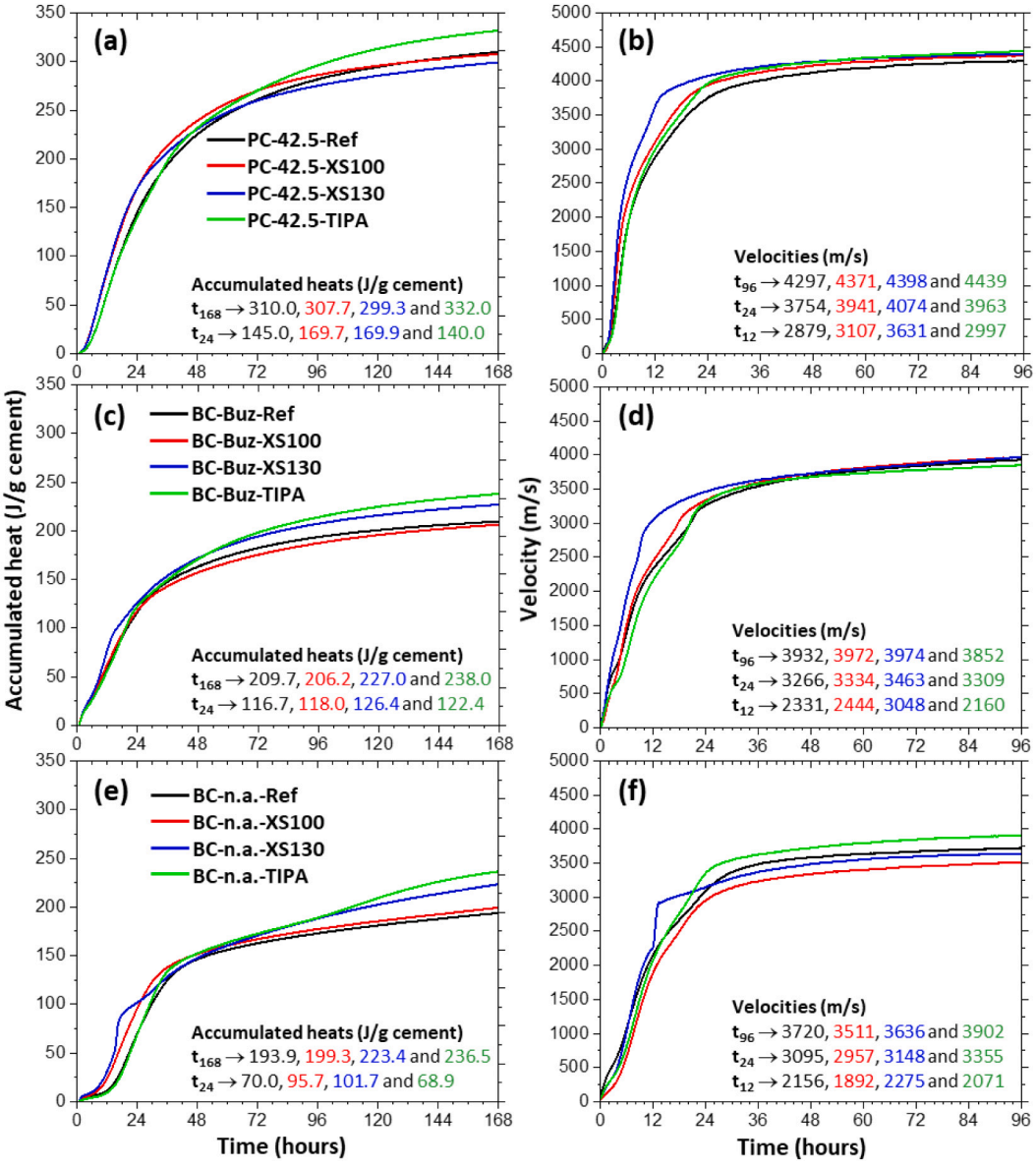

Fig. 2. Calorimetries (of pastes) and ultrasonic pulse velocities (of mortars) for the studied samples displaying the effects of the accelerator admixtures. Left panels: Total heat released curves, normalized to the amount of dried cement during the first week: (a) Portland cement, (c) Buzzi Belite cement, (e) Non-activated Belite cement. The total heats at 24 and 168 h of hydration are given in the insets for comparison. Right panels: Ultrasonic velocity evolutions during the first four days: (b) Portland cement, (d) Buzzi Belite cement, (f) Non-activated Belite cement. The velocities at 12, 24 and 96 h of hydration are given in the insets for comparison.

place at 21 h by UPV and at 34 h by calorimetry. As expected, the alkanolamine-containing admixtures, TIPA and XS130, shows larger aluminate peaks both in calorimetries, see Fig. 3a, and in UPV, see Fig. 3b.

Fig. 2d displays the UPV traces for BC-Buz mortars. In agreement with the slower hydration kinetics, the velocities at 4 days, ~3900 m/s, are lower than those showed by PC-42.5, ~4400 m/s. Moreover, the shape during the acceleration stage is more complex because different hydration reactions are similarly contributing to the connecting network. The acceleration trace for BC-Buz-Ref, see Fig. 3d, shows three maxima at 1.3, 5.9 and 21.2 h likely due to AFt formation from ye'elimite, C-S-H from alite and AFt from C_4AF, respectively. The traces for BC-Buz-Ref and BC-Buz-TIPA mortars are very similar just the aluminate peak at 21 h is enhanced for the TIPA-containing mortar. XS100 slightly accelerates alite and aluminate processes with maxima at 4.9 and 17.8 h, respectively. We interpret this observation as a minor acceleration due to the additional surfaces provided by the C-S-H seed. It is noted that this admixture does not contain alkanolamine and hence, the aluminate process at 17.8 h has smaller area. Interestingly, the XS130 admixture does not importantly change the first two processes but strongly accelerates the aluminate peak which now takes place at 9.1 h and it is evidenced as a sharp peak.

Fig. 2f displays the UPV curves for the BC-n.a. mortars. As expected for this non-activated belite cement, the velocities at 4 days were lower, being 3720 m/s for BC-n.a.-Ref. This figure also shows that XS100 does not accelerate the hydration of the resulting mortar. In fact, it looks like that slightly delay the connectivity development but more studies are needed to confirm this. Concerning TIPA addition, it does not significantly modify the pattern during stage-two but it yields larger velocities during stage-three, very likely due to enhanced C_4AF hydration. XS130 accelerates the hydration at early ages, stage-two, but this not result in larger connectivities at four days. Interestingly, there is a sharp peak at 12.7 h for the acceleration trace of this mortar, see Fig. 3f, which is very similar to the peak observed at 15.8 h in the calorimetry of the

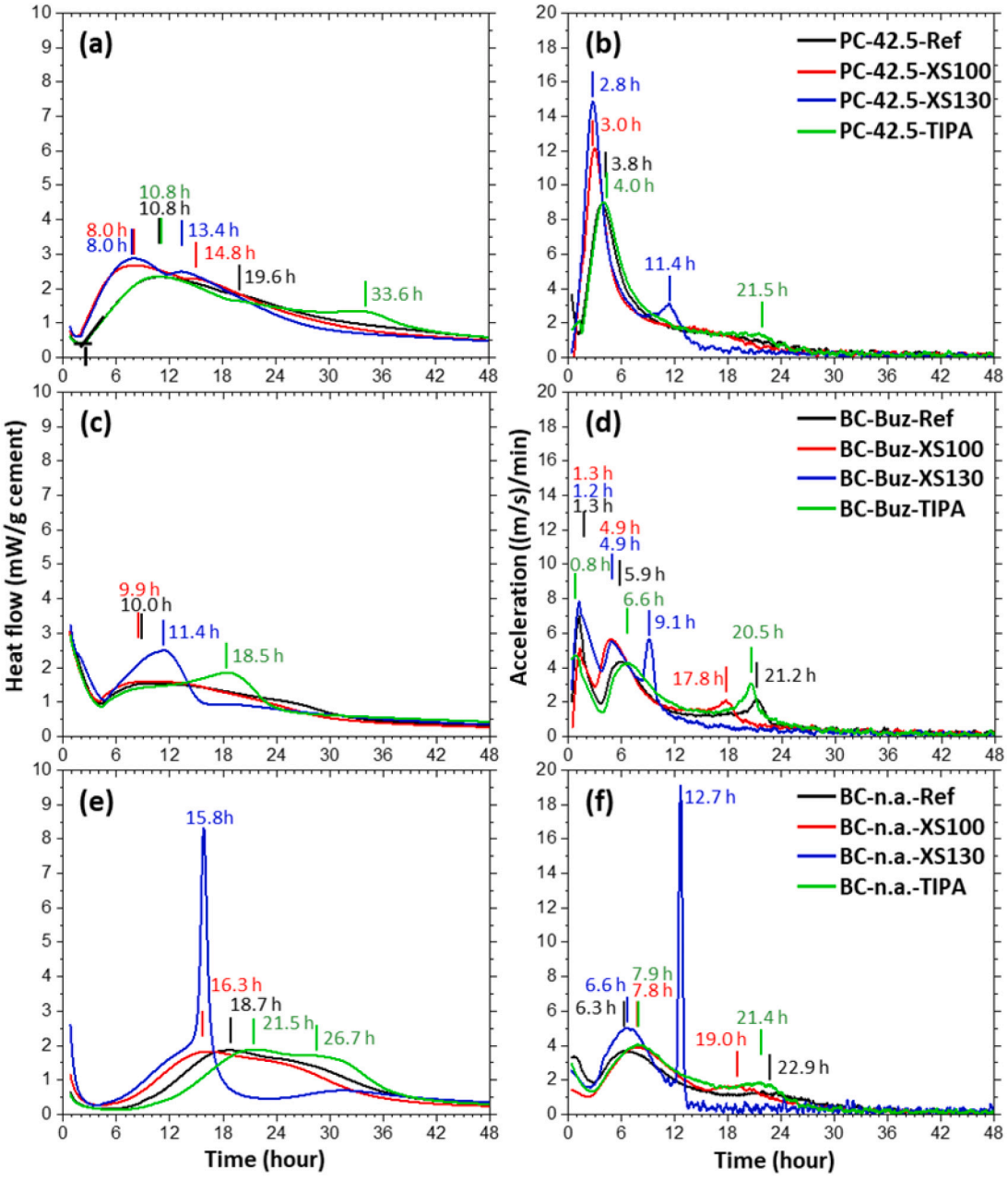

Fig. 3. Heat flow curves of pastes during the first two days for better visualization (left panels) and acceleration of the ultrasonic measurements of mortars (right panels) during the same period of time. (a) Portland cement, (c) Buzzi Belite cement, (e) Non-activated Belite cement. The times for the maxima of the traces are displayed. The times for the maxima in the UPV derivatives are also given in (b) Portland cement, (d) Buzzi Belite cement, (f) Non-activated Belite cement.

corresponding paste, see Fig. 3e. The SXRPD study discussed below will show that these peaks are due to enhanced AFt formation from C_4AF, very likely due the alkanolamine present in this admixture. The agreement in the experimental observations, from three very different techniques, shows the robustness of the employed experimental approaches. Finally, the peaks observed for the BC-n.a. mortars in the acceleration traces, see Fig. 3f, take place earlier than in the corresponding pastes, see Fig. 3f, for the reasons discussed above.

3.4. Mechanical strength characterisation of mortars

Considering the results of the calorimetric study (and to rationalise the efforts minimising the generation of wastes), mechanical strength data were obtained for the three cement mortars containing the XS130 admixture in addition to the neat ones. Moreover, to measure the consequences of all admixtures required large amounts of cements which were not available for BC-Buz and BC-n.a. However, the UPV study for mortars allowed to establish a link between the behaviour of pastes and mortars. An additional mortar, BC-Buz-XS100 was prepared as control, as it contains C-S-H seeds but its early hydration did not release more heat than the reference mortar and the UPV velocity at four days was also very similar to that of the reference sample. It is noted here that the flexural strength values are more difficult to correlate with results from other techniques but they are given here for the sake of completeness. A rheological study for selected mortars was also carried out, see S.I. The objective of this work was to understand if the possible mechanical strength improvements could be due to lower viscosities and hence better specimen compactions. The rheological measurements for BC-Buz-Ref, BC-Buz-XS100 and BC-Buz-XS130 where nearly identical, see S.I.

Fig. 4 displays the compressive and flexural strengths of the studied mortars. It can be seen that the compressive strengths for PC-42.5-Ref are increased notably at early ages when adding the accelerator; 57 % and 27 % at 1 and 7 days, respectively. At 28 days, the compressive strengths are the same within the variability of the measurements. Concerning the flexural strengths, the early age behaviour is similarly mapped out. The addition of XS130 increases the flexural strength 54 % and 11 %, at 1 and 7 days, respectively. At 28 days, it decreases 7 % with the addition of this admixture. It is important to note that calorimetry is a very good technique to quantitatively follow the roles of sulphates, admixtures, *etc.*, within given series and to qualitatively compare with other techniques. However, to use calorimetric data for quantitatively predicting mechanical strength values is very challenging. This is exemplified here by the comparison of the PC-42.5-Ref and PC-42.5-XS130 pastes. At 7 days, PC-42.5-Ref liberated 3.5 % more heat than PC-42.5-XS130 but the mortar with this admixture developed 27 % higher mechanical strength than the reference one. It is explicitly acknowledged that pastes and mortars are compared here, but this is a common practice in cement's field and the role of the same quartz aggregate should not differ too much in the two, very related, systems. It is therefore derived that either reaction(s) releasing less heat are promoted and/or a different microstructure is induced, leading the observed improved mechanical properties. Conversely, the agreement between compressive strength values and the velocities measured by UPV, both in mortars prepared in the same way, is much better. The velocities at 4 days for PC-42.5-Ref and PC-42.5-XS130 were 4297 and 4398 m/s, respectively. Larger velocities for PC-42.5-XS130 reflect higher connectivities which explains the improved mechanical strength data.

For BC-Buz, the compressive strengths of the mortars are increased by the incorporation of the XS130 admixture: 25 %, 15 % and 17 % at 1, 7 and 28 days, respectively. A related behaviour is mapped out by the flexural strength development which increased 8 %, 16 % and 1 % at 1, 7 and 28 days, respectively. It is noted here that the heat developed at 7 days by BC-Buz-XS130 paste is 8 % higher than that of the reference paste and the compressive strength of the mortar is 15 % larger. Fig. 2 also shows that the addition to XS100 does not modify the strength development for BC-Buz. Therefore, the reported increase in compressive strength is likely related to the presence of alkanolamine in XS130. Moreover, the UPV for BC-Buz-XS130 at 1 day, see Fig. 2d, showed the highest velocity and this mortar also showed the highest compressive strength.

For BC-n.a., the compressive strengths are also increased by the addition of XS130: 13 %, 20 % and 13 % at 1, 7 and 28 days, respectively. However, the flexural strengths hardly change with the addition of this admixture, see Fig. 2. This improvement is also likely related to the alkanolamine content of XS130 as discussed just above. Furthermore, it is noted here that the heat developed at 7 days by neat BC-n.a. and BC-Buz pastes were 209 and 210 J/g. However, the compressive strength values of the corresponding neat mortars at this age were 14.3 and 27.4 MPa, respectively. As expected, the agreement between the UPV measurements and the compressive strengths is much more satisfactory. The velocities at four days for BC-n.a. and BC-Buz mortars were 3720 and 3932 m/s, respectively. Larger velocities are related to larger compressive strength at seven days. Moreover, the heat developed at this age with the addition of the admixture by BC-n.a. and BC-Buz pastes were 239 and 227 J/g, respectively. Nevertheless, the compressive strengths of the corresponding mortars are 17.1 and 31.6 MPa, respectively. Again, it is not straightforward to derive quantitative values of mechanical strengths from the calorimetric data.

3.5. *Ex situ thermal analysis study*

Fig. 5 shows the thermal analysis curves for the 27 investigated pastes (hydration-arrested). For the sake of conciseness, the portlandite contents, derived using the tangential method [63], and the overall weight losses are also given in the Fig. 5. The portlandite contents are referenced to the pastes containing the free water, *i.e.* neat pastes, for direct comparison with the RQPA results reported in the next subsection. These portlandite contents are calculated as follow: 1) the weight loss is obtained by the tangential method, 2) this value is converted to weight percent of portlandite using the 4.11 factor (74.09 $gmol^{-1}$/18.02 $gmol^{-1}$), and 3) as the thermal analysis value is referred to the arrested sample, the previous percentage is normalized to 100 g of neat paste by multiplying it by the correction factor: 1 − FW(%) / 100. Table S5 compiles the main values derived from the thermal study.

Several observations can be drawn from the analysis of the data reported in Fig. 5. Firstly, and as expected, the overall weight losses increase with hydration time in the nine series. Furthermore, and also as expected, in the absence of pozzolanic reaction(s), portlandite contents increases with time in eight out of the nine series. For BC-n.a.-TIPA, the traces showed a slightly lower amount of CH at seven days than at 2 days. We interpret this due to the inherent (minor) variability of the experimental procedures. In any case and taking all together, the results show the high robustness of the experimental methods used here.

Secondly and interestingly, for the PC-42.5 pastes, the CH contents (at the same hydration ages) are smaller in the series using the admixtures, mainly PC-42.5-XS130. This is observed in spite that the overall weight losses are larger for the pastes with the admixtures. This result can be interpreted in two ways: i) the hydration of C_3S is delayed in the pastes containing these admixtures; and/or ii) there is an additional consumption of CH due to enhanced formation of AFm-Hc. In any case, it is noted that the pastes with the XS130 admixture show the largest overall weight losses within each series. It should be noted that alkanolamines, present in XS130, are known to accelerate the hydration of aluminates [24,64] and thus enhanced formation of AFm is expected.

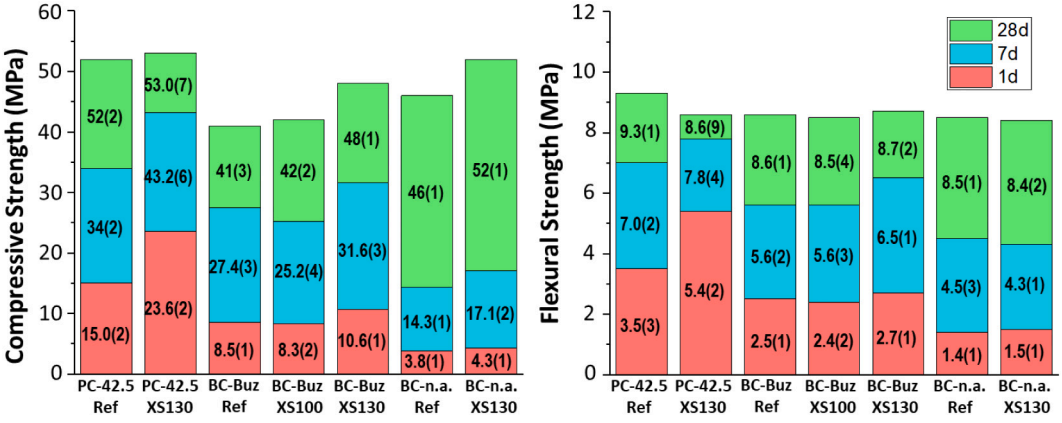

Fig. 4. Mechanical strength data for the studied mortars as function of time and the accelerators. Compressive strength (left panel). Flexural strength (right panel).

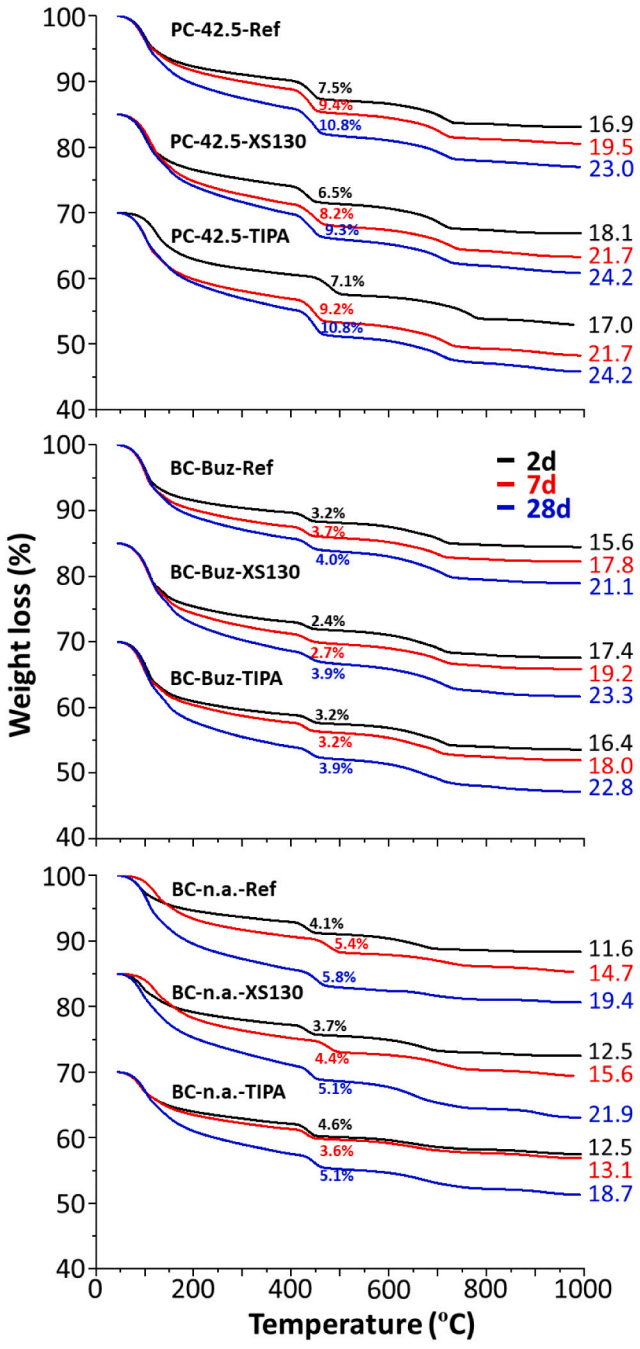

Fig. 5. Thermal analysis data for all studied pastes after arresting the hydration and isothermal heating at 40 °C for 30 min. The traces for the different series have been displaced vertically for better visualization. However, the traces for the series just as function of the hydration time have the same origin, *i.e.* they are not displaced. The CH contents (wt%) are referenced to the pastes containing the free water for a direct comparison to the RQPA data given in Tables 1–3. The total weight losses (wt%), after arresting the hydration, are also shown.

Thirdly, this feature, slightly less CH in the admixture-containing pastes, is also shown by BC-Buz and BC-n.a., see Fig. 5. The difference between the portlandite contents of the reference pastes and the admixture-containing pastes is larger at early ages, *i.e.* 2 and 7 days, than at 28 days where the differences are almost negligible. This observation points towards a delay in the silicate hydration reaction(s) more than a significant change of the C-S-H gel composition.

Fourthly, from this thermal study the free water (FW) contents can be derived, as detailed in the experimental section and complemented in the S.I. These values are reported in Tables 1–3 together with the RQPA results. Alternatively, the combined water fraction [65] is obtained from the nominal water content and the measured FW values.

Finally, it should be noted that there is a better agreement between the mechanical strength developments and the FW contents (or alternatively the combined water fractions) than with the calorimetric data. For instance, the FW contents for PC-42.5-Ref and PC-42.5-XS130 at 7 days are 21.4 % and 19.4 %, respectively. Therefore, PC-42.5-XS130 which displayed higher mechanical strengths has higher combined water fraction than PC-42.5-Ref although it released less hydration heat. This point towards a change in the hydration reactions which are explained in the powder diffraction studies, both *ex situ* by LXRPD and more detailed by the *in situ* SXRPD study.

3.6. *Ex situ laboratory powder diffraction characterisation*

The LXRPD patterns for the 27 pastes were collected by adding an internal standard, quartz, to derive the overall amorphous and crystalline-non-determined (ACn) contents [47,66]. Figs. S3 and S4 give, as examples, the Rietveld plots, after 28 days, for the three reference pastes (without admixtures) and the three pastes with XS130, respectively. All raw data are openly deposited and hence any interested reader could download them, see data availability subsection below.

The LXRPD data were evaluated by the Rietveld methodology and using an internal standard. This allows to derive the Rietveld quantitative phase results which are gathered in Tables 1, 2 and 3 for the three overall series, PC-42.5, BC-Buz and BC-n.a., respectively. The tables also report the FW determined from the thermal studies, see above, and the calculated contents for C-S-H gel, additional amorphous phases and FW according to the chemical reactions given in the S.I. The results will be discussed in three stages: i) dissolution of the anhydrous phases, ii) crystallisation-precipitation of hydrated products, and iii) comparison of the obtained data with the calculated ones from the assumed chemical reactions.

3.6.1. *PC-42.5 pastes*

Table 1 reports the results for the admixture activation of the PC. Concerning the evolution of the anhydrous phases: 1) The C_3S hydration degree increases from ~60 % to ~90 % from 2 to 28 days and, in this time frame, it does not significantly change with the addition of admixtures. 2) For this PC which contains a low amount of belite, C_2S does not significantly hydrate in the first 28 days. In fact, it seems that its relative amount increases with time, which has no physical meaning. We interpret this result as lower amounts of alite interfere less with the belite fitting, both phases have strong diffraction peak overlapping, resulting in belite phase being underestimated. The dissolution of alite, which results in lower overlapping, yields powder patterns where belite phase is better analysed. This possible belite underestimation at t_0, ~2 wt%, has not been considered in order not to further complicate the analyses. From data in Table 1, it can be derived that the studied admixtures do not accelerate belite hydration. 3) Concerning the hydration degrees of C_4AF, in PC-42.5-Ref this phase reacts 50 % at 28 days. TIPA slightly reduces its reactivity, down to 30 %, meanwhile XS130 slightly increases, up to 60 %. 4) The hydration degrees of C_3A increase from ~40 % at 2 days to ~80 % at 28 days and TIPA does not significantly change them. However, XS130 accelerates its hydration at early ages.

Concerning the evolution of the hydrated products, some observations can be made. 1) PC-42.5-Ref showed larger amounts of portlandite at the three ages, when compared to the admixture containing pastes. The CH percentages from RQPA, see Table 1, are a bit larger than those derived from the TA, see Fig. 3. This could be due to the usage of the tangent method in the TA study, which may slightly underestimate CH content. Furthermore, PC-42.5-XS130 is the paste with the lower amount of crystalline portlandite at 28 days by RQPA. The trend is in agreement with the thermal analysis data reported above. These data are

consistent with a somewhat slower hydration kinetics of C_3S at early ages for PC-42.5-XS130. However, at 28 days the hydration degree of C_3S is slightly larger but the portlandite content slightly lower. In this respect, the formation of Hc and Mc phases also consumed small amounts of CH. It must also be noted that the possible underestimation of belite/alite ratio at the initial time could also contribute to the measured relatively low CH content. In other words, if the pristine PC sample has 31.3 wt% of alite and 7 wt% of belite, a lower reaction degree of C_3S is derived compatible with the measured CH content. 2) The crystalline ettringite contents are larger for PC-42.5-XS130 and lower for PC-42.5-TIPA, at all ages, when compared to the reference PC paste. 3) Concerning the crystalline hemi- (Hc) and monocarbonate (Mc) contents, it seems that the admixtures slightly increase their percentages. 4) In agreement with an increase calcium aluminate reactivities, and hence ettringite crystallisation, PC-42.5-XS130 is the paste with the lowest FW contents at the three ages and hence, the larger combined water fractions. At 7 days, the FW values for PC-42.5-XS130 and PC-42.5-Ref are 19.4 and 21.4 %, respectively. Thus, it becomes clear, in agreement with an earlier report [65], that the combined water fraction is a good descriptor for correlating the mechanical strengths values.

On the one hand, Table 1 also reports the calculated C-S-H contents obtained as the average from the C_3S dissolution and the portlandite crystallisation by assuming a fixed stoichiometry: $(CaO)_{1.8}SiO_2{\cdot}4H_2O$. This is the stoichiometry with the water content of C-S-H at the micro-scale [67], volume sizes between ~0.3 to ~5 μm^3, which implies that the 'gel pore water' is considered within the combined water fraction. This is a coarse approximation and it helps to explain that measured FW contents by TA are higher than those obtained from the calculations. Furthermore, this disagreement increases as the C-S-H content increases, see Table 1. However, by considering the C-S-H stoichiometry as $(CaO)_{1.8}SiO_2{\cdot}1.8H_2O$ [68], *i.e.* excluding all gel pore water, the calculated FW contents for PC-42.5-Ref are 25.8, 22.8 and 20.7 % at 2, 7 and 28 days, respectively. Now, these values are higher than the obtained ones from TA, *i.e.* 23.3, 21.4 and 18.1 %. Therefore, we conclude that roughly, 50 % of the gel pore water of C-S-H is lost in the isothermal treatment for 30 min at 40 °C. In other words, approximately half of the C-S-H gel pore water is considered within the coined term "combined water fraction" [65]. On the other hand, and as expected, the overall amount of amorphous phases is higher than the C-S-H content. This is due to the existence of other amorphous phases like Fe—Si hydrogarnet, amorphous AFm phase(s), *etc.* All these components are summed up within the black box coined 'other ACn', see Table 1.

3.6.2. BC-Buz pastes

Table 2 reports the results for the admixture activation of the BC-Buz. 1) The reaction degrees of C_3S were quite close to those reported for PC-42.5 at the corresponding ages. It seems that XS130 slightly delayed C_3S reactivity at early age, *i.e.* 2 days. 2) C_2S is clearly more reactive in this cement as it reacts ~40 % at 28 days in BC-Buz-Ref. We justify this observation because belite phase was chemically activated by sulphur during the clinkering stage. XS130 further increases belite reactivity at intermediate hydration ages. Conversely, it seems that TIPA slightly delays belite reactivity. 3) The hydration degrees of C_4AF in the reference cement are larger than those measured for PC-42.5-Ref. We justify this enhanced reactivity because the lower clinkering temperatures of BCs lead to smaller grain sizes for the aluminate phases and hence their reactivities increase. Furthermore, XS130 notably accelerates C_4AF hydration at early ages which is maintained at later ages. TIPA also seems to accelerate C_4AF hydration at early ages.

Concerning the evolution of the hydrated products, it is again observed larger amounts of CH at the three ages in the reference BC-Buz pastes, when compared to the admixture-containing ones. This is in line with the thermal analysis results. BC-Buz-XS130 showed larger amounts of ettringite at 2 and 7 days but not at 28 days. This sample showed larger overall amount of Hc and Mc than the reference paste. This behaviour is more evident for BC-Buz-TIPA where lower AFt contents are measured but larger contents of Hc and Mc were determined. It should also be noted that the FW contents determined by thermal analysis are a bit larger than those obtained in the related PC pastes because belite reactivity is slower. In any case the FW contents evolved as expected and BC-Buz-XS130 had the larger combined water fractions, *i.e.* the lower FW contents, for the three studied ages.

The calculations show that the amounts of C-S-H gel are lower when compared to PC pastes because the overall smaller reactivities of the calcium silicates. Intriguingly, the agreement between the FW contents calculated from mass balance calculations and the ones derived from thermal analysis are much closer for BC-Buz than those for PC-42.5. This may indicate that the gel-pore water is more retained in the BC pastes.

3.6.3. BC-n.a. pastes

Table 3 reports the results for the admixture activation for BC-n.a. 1) As observed before, it seems that the admixtures slightly delay C_3S reactivity at very early ages. Moreover, the reaction degrees of C_3S, at a given age, were slightly larger than those of PC-42.5-Ref and BC-Buzz. 2) C_2S does not significantly react in any of the three pastes up to seven days. At 28 days, XS130 accelerates belite hydration, meanwhile TIPA could delay it. 3) XS130 accelerates C_4AF hydration at all ages but TIPA seems to retard it at early ages and accelerate it at later ages.

It is also observed larger amounts of portlandite in the reference BC-n.a. pastes when compared to the admixture-containing ones. The ettringite contents do not change significantly by the admixture addition neither the crystalline Hc contents. For this series, the FW of BC-n.a.-XS130 is not significantly lower than those of the reference pastes. The higher C_4AF hydration degree in BC-n.a.-XS130 at 28 days combined with a similar FW content and a larger mechanical strength development, see Fig. 2, may indicate that the amorphous Fe—Si hydrogarnet resulting from C_4AF hydration may have good binding properties.

Interestingly, and in agreement with the BC-Buz behaviour, the FW contents estimated by mass balance calculations and the ones derived from thermal analysis show good agreement, better than in the PC pastes. This again may suggest a larger gel pore water retention for C-S-H gels in BC pastes.

3.7. In situ synchrotron powder diffraction characterisation

The SXRPD patterns were collected as soon as possible after mixing, ~20 min, and at that time $C\bar{S}H_{0.5}$ was always fully dissolved. For optimising the synchrotron beamtime, the next ~3 h (induction period) were employed to acquire data on different samples, and then, the *in situ* data collection was continued up to ~20 h. Two final datasets were taken at ~50 h for PC-42.5 and BC-Buz and for the same capillaries. For BC-n.a., data were continuously collected up to ~37 h. It should be noted that different calcium sulphates have different solubilities which can affect to the aluminates early age reactivity as previously reported [26], however this parameter space has not been addressed here.

Selected SXRPD raw data are shown in Figs. S5 to S7 to illustrate the change in the powder diffraction patterns. All diffraction data for the ten pastes were analysed by the Rietveld method to extract quantitative values. To develop and present a unified picture, mineralogical quantitative data are displayed grouped as developing phase (dissolution or crystallisation) rather than showing the evolutions of the different cements. Following this premise, Fig. 6 shows the dissolution of the sulphate carrier ($C\bar{S}H_2$ for PC-42.5 and BC-n.a. and $C\bar{S}$ for BC-Buz) and the crystallisation of AFt. It can be seen for PC-42.5 and BC-n.a., that the amounts of $C\bar{S}H_2$ are higher at 20 min than at t_0. This has been previously observed, see for instance [26], and it is due to the fast dissolution of bassanite with the subsequent secondary gypsum crystallisation.

Concerning the calcium sulphate dissolutions, TIPA does not significantly alter the dissolution rates. However, it can be seen that XS100 accelerates them. Furthermore, XS130, which contains similar C-S-H

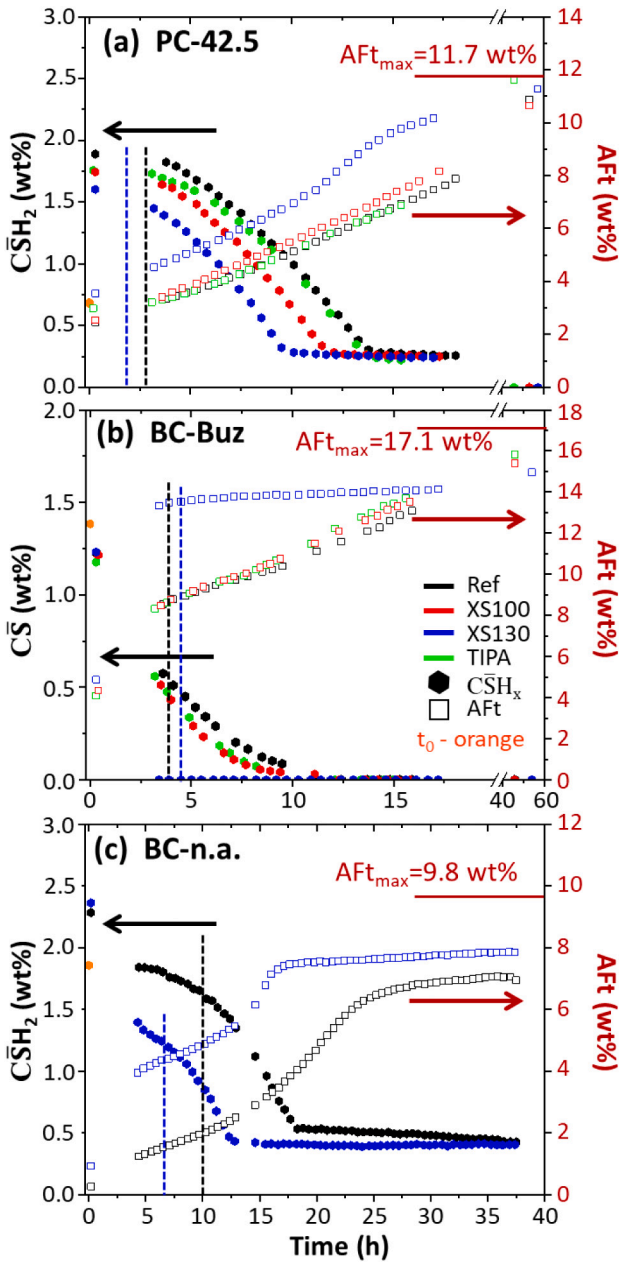

Fig. 6. Phase content evolutions with time from *in situ* SXRPD. (Left) Dissolution of the sulphate carrier. (Right) Crystallisation of ettringite. The maximum amounts of AFt, considering SO_3 as the limiting reactant, are also displayed. The vertical (dashed) lines depict the end of the induction periods for the corresponding pastes.

nanoparticles but additional alkanolamines, strongly accelerates sulphate dissolution. This is more conspicuous for BC-Buz-XS130, see Fig. 6b, where solid calcium sulphates are depleted as soon as at 4 h. Therefore, a synergistic effect between the seeding and the alkanolamines takes place for sulphate dissolution. We explain this enhanced sulphate dissolution rate because the additional C-S-H nanoparticles adsorb sulphate anions, displacing the chemical reaction. However, the mechanism of this synergistic effect is not known. We speculate that the organic species could contribute to have less agglomeration of C-S-H nanoparticles and therefore more available surface for adsorption, and/or, aluminium could be complexed increasing its availability for ettringite crystallisation, and hence, indirectly favouring further sulphate dissolution. More research is needed to understand the mechanism.

Regarding AFt crystallisation, XS100 and TIPA do not seem to accelerate this process, see Fig. 6. However, XS130 strongly accelerates AFt crystallisation at very early ages. Interestingly, for PC-42.5, the addition of XS130 resulted in an accelerated AFt crystallisation at ~14 h, see Fig. 6a. This process coincides with the small shoulder to the right of the main peak in the calorimetric study, see Fig. 3a, and with the peak seen in the UPV trace of the corresponding mortar at 11.4 h, see Fig. 3b. Hence, this small heat flow peak is due to an enhanced AFt crystallisation (or accelerated C_3A dissolution, see below) and not due to a partial AFt to AFm conversion. At this hydration age, *i.e.* 14–16 h, this paste still contains undissolved gypsum and no AFm-type phases. Moreover, and for many pastes, AFt keeps crystallising without any crystalline calcium sulphate dissolution. These sulphates should come from an amorphous reservoir, likely the C-S-H nanoparticles. It is noted here that enhanced sulphate availability, and therefore their possible adsorption at C-S-H gel, may provoke important changes in the morphology of the growing nanoparticles [69,70]. Fig. 6 also displays the theoretical amount of AFt expected from complete crystallisation considering SO_3 as the limiting reactant. It can be seen that at ~2 d, the SXRPD derived values are quite close to those values, but those obtained from LXRPD, see Tables 1–3, are significantly smaller. This is likely due to the arresting hydration step carried out for the LXRPD study which is known to partly decompose crystalline ettringite.

Fig. 7 shows the C_4AF dissolution patterns for the 10 studied pastes. For PC-42.5, the admixtures do not significantly enhance C_4AF dissolution at very early ages. At 2 days, the two pastes containing alkanolamines displayed higher C_4AF dissolution. For BC-Buz and BC-n.a., XS130 increases C_4AF hydration from the very early ages. This again shows the synergistic effect of C-S-H seeding and alkanolamines as neither XS100, nor pure TIPA, show this behaviour. Furthermore, BC-n.a.-XS130 showed a surge in C_4AF dissolution at ~15 h, see Fig. 7c, which coincides with the jump in AFt crystallisation, Fig. 6c. These two features explain the sharp peaks centred at 16 h (for the calorimetry of the paste) and at 13 h (for the UPV of the mortar), see Fig. 3e and f, respectively. Hence, the sharp peaks observed in the calorimetric and UPV studies for BC-n.a.-XS130 are due to a sudden increase of C_4AF dissolution, with solid gypsum still not depleted, see Fig. 6c. Fig. 7 also displays the theoretical (expected) AFt crystallisation from the amount of aluminium which dissolves according to the SXRPD. It can be seen that the shape of the traces agrees very well with the determined ones for AFt crystallisation. However, the values are smaller which suggest the dissolution of amorphous calcium aluminates at very early hydration ages.

Fig. 8 displays the C_3A dissolution patterns for PC-42.5 and additionally $C_4A_3\bar{S}$ for BC-Buz. This Figure does not have a panel for BC-n.a. since this cement does not contain C_3A neither $C_4A_3\bar{S}$. For PC-42.5, the studied admixtures did not increase C_3A dissolution much at very early ages, see Fig. 8a. However, again at two days the pastes containing alkanolamines showed enhanced C_3A dissolution. In addition, BC-Buz-XS130 displayed accelerated C_3A dissolution from very early ages. Fig. 8 clearly shows that C_3A dissolution, as well as that of $C_4A_3\bar{S}$, is accelerated in BC-Buz-XS130. Fig. 8 also shows Hc crystallisation evolution. For the four PC-42.5 pastes, Hc is only measured at t ~ 50 h when solid calcium sulphates are depleted, see Fig. 6a. A similar behaviour is shown by three pastes from BC-Buz, see Fig. 8b. The Hc contents after two days are significantly larger for the pastes containing TIPA and XS130 than for the reference and XS100-containing pastes, which correlate with enhanced calcium aluminate(s) dissolution. Moreover, for BC-Buz-XS130, Hc crystallisation started from very early hydration ages, *i.e.* ~3 h, which is consistent with the observed calcium sulphate depletion, see Fig. 6b.

Fig. 9 shows the C_3S dissolution patterns. For PC-42.5, TIPA does not modify C_3S hydration. Furthermore, XS100 and XS130 seeding increases C_3S reaction very slightly, see Fig. 9a. This behaviour is fully mirrored by the CH crystallisation, also displayed in that Figure. Therefore, it is

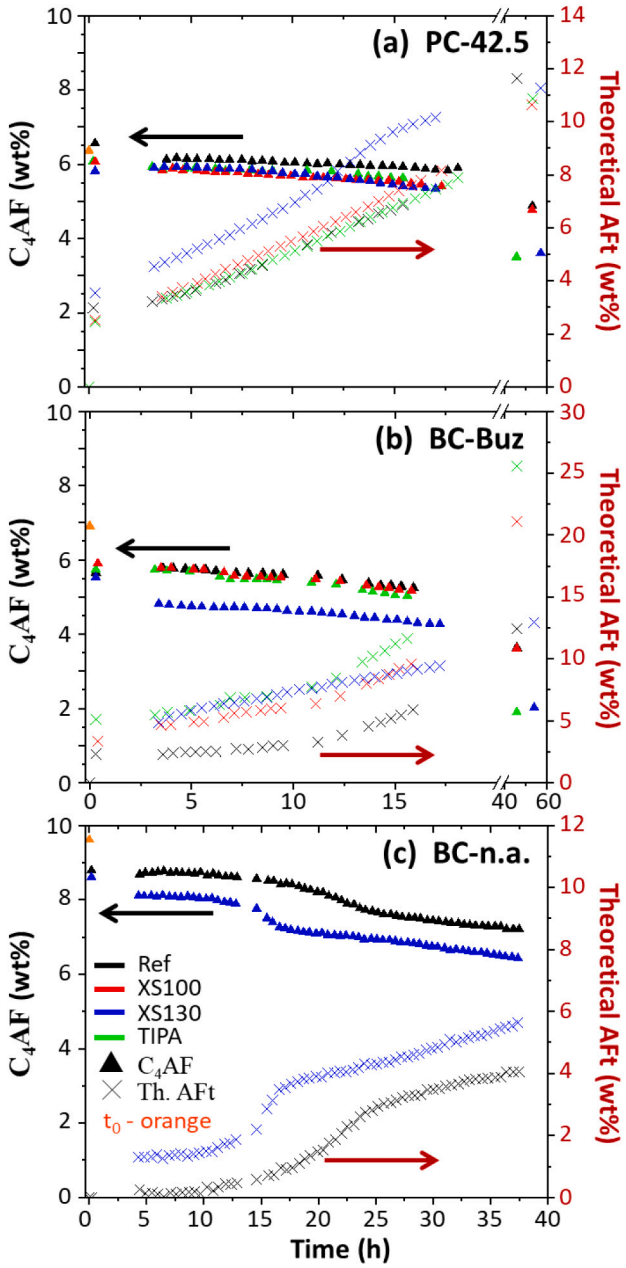

Fig. 7. Phase content evolutions with time from *in situ* SXRPD. (Left) Dissolution of C_4AF. (Right) Theoretical amount of ettringite from the dissolutions of the crystalline aluminium-containing clinker phases.

concluded that C-S-H particle seeding accelerates PC hydration but it does not significantly activate alite reaction in the studied PC. C-S-H seeding add appropriated surface for sulphate (and subsequently) aluminate adsorption enhancing the dissolution of these phases at very early ages. In any case, pore solution measurements are needed which were not within the scope of the present work.

Fig. 9b displays the C_3S dissolution for the four BC-Buz pastes. In this case TIPA and XS100 do not accelerate C_3S reaction significantly at very early ages but XS130 does. However, and interestingly, the hydration rate of C_3S for BC-Buz-XS130 is slower between 5 and 15 h, see Fig. 9b. We explain this behaviour because the enhanced aluminate dissolution may result in more Al^{3+} species adsorbed in the C-(A)-S-H gel which is known to hinder C-(A)-S-H nucleation and growth [71–73]. This could be possible even if the limiting reaction is C_3S dissolution because the coupling of the reactions [30,32].

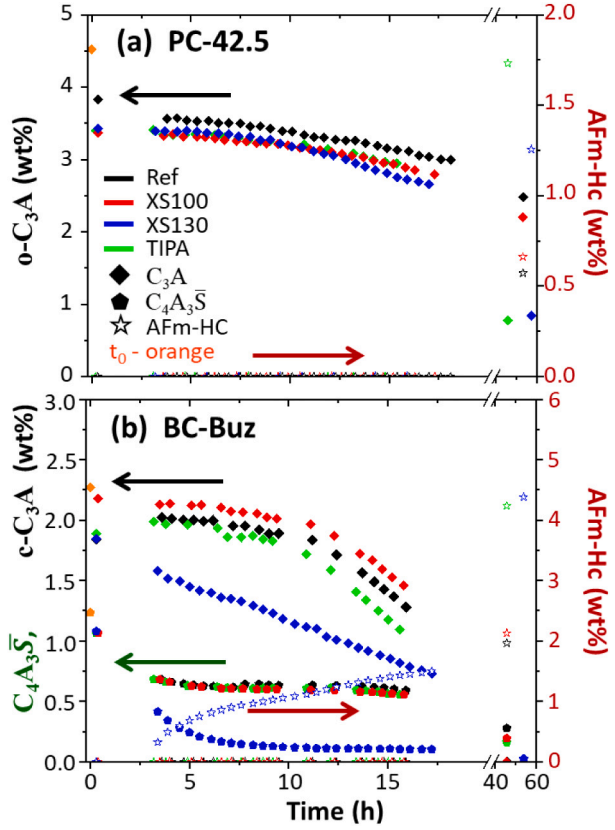

Fig. 8. Phase content evolutions with time from *in situ* SXRPD. (Left) Dissolution of C_3A and $C_4A_3\bar{S}$. (Right) Crystallisation of Hemicarbonate, Hc.

CH crystallisation is also displayed in Fig. 9b. The measured CH contents for BC-Buz-TIPA and BC-Buz-XS100 are only marginally larger than those of the reference paste. However, the evolution of the CH content for BC-Buz-XS130 is much slower, see Fig. 9b. This was expected as the crystallisation of Hc for this sample, see Fig. 9b, consumes CH.

The hydration of alite for BC-n.a. pastes is displayed in Fig. 9c. On the one hand, it can be observed that XS130 slightly accelerates C_3S hydration at very early ages. However, there is a crossover, and after ~23 h, the amount of hydrated alite in BC-n.a.-XS130 is slightly smaller than that in BC-n.a.-Ref. This behaviour, as discussed above, is again justified by the enhanced aluminate dissolution that takes place in BC-n.a.-XS130 which may result in more aluminate species being adsorbed in the C-S-H gel nanoparticles. This adsorption could be the reason for the slowdown of the hydration reaction but more research is needed to explain the observed behaviour. On the other hand, CH evolution fully mirrors the alite reactivity. This was expected as there is not consumption of CH by any chemical reaction, *i.e.* AFm-type phase formation, *etc.* This observation highlights the high robustness of the employed experimental procedures for data collection and data analysis.

Fig. 10 displays the C_2S contents with hydration time. For PC-42.5 and BC-Buz pastes, the addition of the studied admixtures did not change the observed behaviour, *i.e.* absence of any reactivity in the first two hydration days. In fact, for PC-42.5 pastes at 2 days, it seems that belite contents have increased. This cannot be and a possible origin for this behaviour was already discussed above. For BC-n.a., it looks like XS130 has slightly increased belite reactivity. This observation is constant with hydration time and it could be within the variability/errors of the analyses. Finally, Fig. 10 also displays the calculated C-S-H gel contents from the dissolution of the silicates and the formation of CH. These results are shown for consistency and the values at the latest hydration ages for PC, BC-Buz and BC-n.a. are ~22, ~12 and ~11 wt% which are in good agreement with the RQPA from LXRPD at two days,

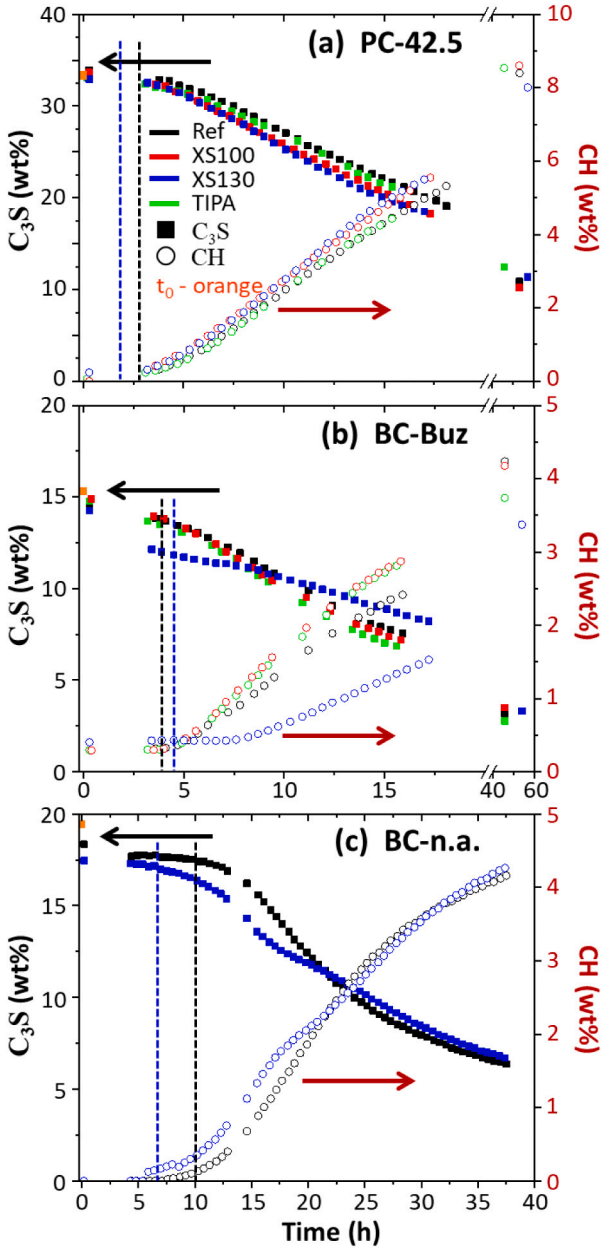

Fig. 9. Phase content evolutions with time from *in situ* SXRPD. (Left) Dissolution of C_3S. (Right) Crystallisation of CH. The vertical (dashed) lines depict the end of the induction periods for the corresponding pastes.

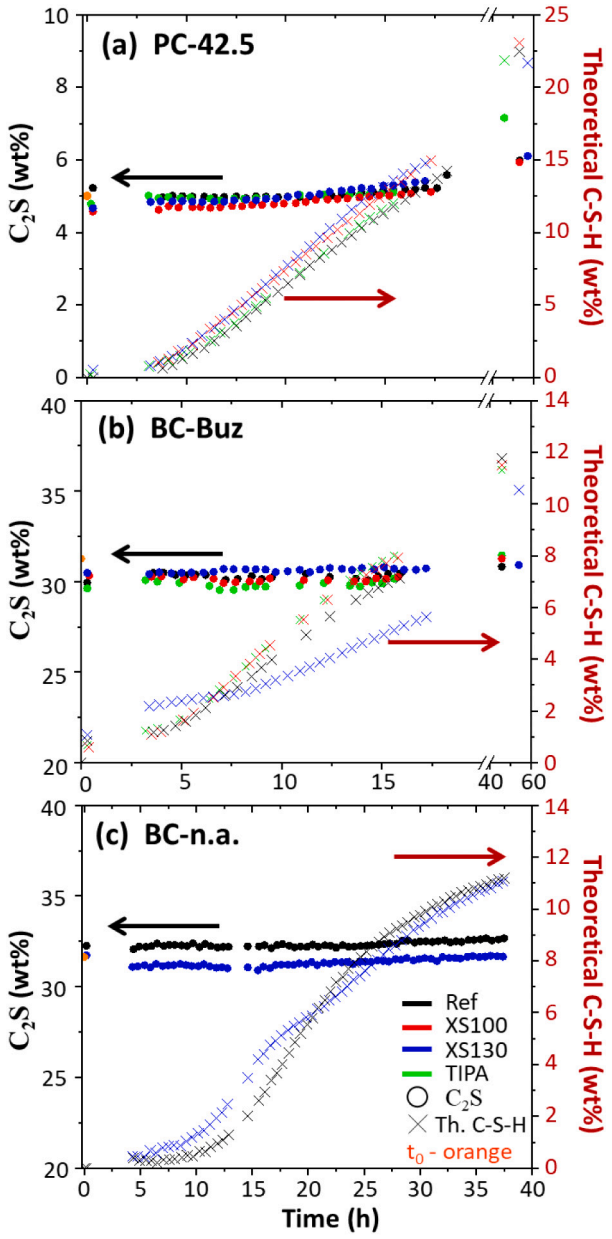

Fig. 10. Phase content evolutions with time from *in situ* SXRPD. (Left) Dissolution of C_2S. (Right) Theoretical amount of precipitated C-S-H gel.

~21, ~9 and ~14 wt%, respectively, see Tables 1–3.

4. General discussion

4.1. Advantages and limitations of the employed techniques

The heat flow curves obtained in any calorimetric study are compound functions of the different hydration reactions which develop simultaneously in the hydrating binders. This characterisation is simple, widely-available and very useful to test overall effects like modification of the induction periods or the increase of total heat released at given early hydration times. However, to extract mechanistic information from the overall curves, for multimineral cements, is very challenging. Additionally, ultrasonic pulse velocities allow to *in situ* measure the connectivity development of pastes [74] and mortars when using accelerators. Moreover, this technique permits continuous microstructure monitoring without any sample preparation. In any case, these two approaches are not phase-selective but overall responses are obtained. Conversely, *in situ* powder diffraction can reveal the hydration of every crystalline phase. However, this technique, when based on laboratory sources, are prone to experimental errors like overlapping of diffraction peaks, high preferred orientation of some phases like portlandite and calcite, lack of random particle orientations in all diffraction directions, water bleeding when using reflection configuration, *etc.*, complicating the extraction of accurate results. In this case, the backing from additional tools like thermal analysis, thermodynamic modelling, *etc.*, is highly desirable. *In situ* high-resolution synchrotron powder diffraction minimises most of the problems faced by LXRPD but it is not widely-available and it requires certain expertise. Moreover, the mechanical strength values can be related to the development of hydrating phases. However, a limitation for quantitatively predicting the mechanical strength of mortars is the important role of the microstructure, including but not restricted to, pore refinement, homogeneous C-S-H distribution

and the interfacial transition zone features. This can be partly mitigated by employing UPV measurements where the microstructural evolutions can be followed.

4.2. C-S-H seeding and the induction period

During the induction periods shown in Fig. 3a and b by calorimetry and UPV measurements, respectively; *in situ* SXRPD clearly shows that sulphates keep dissolving, see Fig. 6. Furthermore, Fig. 6 also demonstrates that ettringite keeps crystallising. Therefore, the term ⟨dormant period⟩ which is still widely used, even in quotes (see for instance [29]), should be avoided. C-S-H seeding normally shortens the induction period, as measured by calorimetry and UPV, but this is not necessarily the case for all type binders as shown for BC-Buz-XS130.

4.3. C-S-H seeding of PC

This work demonstrates that the hydration of the studied PC, in the employed realistic conditions, is accelerated but the hydration of the alite phase is not significantly enhanced at very early ages.

4.3.1. C-S-H seeding of alite phase vs. PC

This work contributes to explain the different behaviour of C-S-H seeding for alite (pure phase) hydration and PC hydration. It is noted that the hydration of seeded alite pastes takes place in the absence of meaningful amounts of sulphate and aluminium ions. Conversely, the hydration of seeded PC pastes takes place in an enhanced sulphate and aluminate hydration media. These ions are known to modify the nucleation and growth kinetics of C-(A)-S-H.

4.3.2. C-S-H seeding and sulphate balance

C-S-H seeding, mainly when alkanolamine are also employed, seems to shift the equilibria by adsorbing SO_4^{2-}. Alkanolamines enhance Al^{3+} in pore solution which strengthens ettringite precipitation, resulting in further dissolution of calcium sulphate(s). This observation is important because it implies that the use of this type of accelerating admixtures may require higher content of sulphates.

4.3.3. Phases reactivities

Combining the results from the calorimetric study, the UPV investigation and the *in situ* synchrotron powder diffraction, it can be deduced that the shortened induction period in this PC, when using X-Seed 130, is related to enhanced AFt crystallisation and not to faster C_3S dissolution. Moreover, the acceleration of the PC hydration after C-S-H seeding being related to AFt enhanced crystallisation, and not to faster C_3S dissolution, is in line with the geochemical theory of dissolution of C_3S [75] where alite dissolution is the rate-limiting reaction. Moreover, we speculate that our findings do not back the passivation layer theory for the justification of the induction period as (partly) moving away the C-S-H precipitation has not accelerated alite hydration in the two studied PC pastes containing C-S-H seeds, PC-42.5-XS100 and PC-42.5-XS130. However, spatially-resolved techniques are needed to directly and accurately address this topic.

4.4. C-S-H seeding of BCs

In spite of the belite cement hydration acceleration, here it is shown that belite phase hydration is not significantly accelerated at early ages by C-S-H seeding.

4.4.1. Phase reactivities

Belite (phase) hydration has been only to a minor extent accelerated by XS130 seeding. Alite could initially react a bit faster but the *in situ* synchrotron study has demonstrated that a slowdown of its hydration takes place, see Fig. 9b and c, being even slower than that occurring in unseeded media after about 10–12 h. Enhancing sulphate [69,70] and aluminate [26,71–73] dissolutions may result in delayed C-S-H growth (which is evidenced as retarded C_3S hydration). The improved mechanical properties of the C-S-H seeded BCs are assigned to enhanced aluminate C_4AF and C_3A hydration.

4.4.2. Coupled reactions

Interestingly, the start of the main hydration peak period for BC-Buz-XS130, *i.e.* 4.8 h, is retarded when compared to that of BC-Buz-Ref, 4.3 h, see Fig. 3c, as detected by calorimetry. This unusual behaviour could be due to the enhanced sulphate and aluminate dissolution rates, see Figs. 6b and 8b, respectively. More available Al^{3+} cations, because the alkanolamine presence, could be adsorbed at the surfaces of the C-S-H seeds modifying the nucleation and growth pattern of C-(A)-S-H [69–73]. This is transferred through the pore solution to the alite dissolution which may result in a slightly slower rate of hydration, Fig. 9b. In other words, the enhanced dissolution of sulphates and aluminates, releasing less heat of hydration, may slowdown alite hydration. The resulting overall picture is a slightly delayed cement hydration by calorimetry, which is indeed not the case as demonstrated by the *in situ* SXRPD study. It is also noted here that gypsum has been reported to moderately enhance the hydration of C_3S and C_3S/C_3A model mixtures [76], highlighting the difficulties of transferring pure phase results to the hydration of commercial cements, where several reactions simultaneously take place.

The measurements reported here may contribute to understand previously counterintuitive observations. For instance, C-S-H seeding was shown to accelerate C_3S hydration as measured by the micro-reactor technology [77] but with the same approach it did not accelerate, in fact retarded, PC-slag hydration in alkaline media [78]. We speculate that in last case, C-S-H seeding firstly enhances aluminate dissolution, and if the aluminate species are not removed from the hydrating media, they delay silicate hydration which was the final observation.

4.5. Synergy of C-S-H seeding with alkanolamines

Synergistic effect(s) has been clearly observed when employing C-S-H seeding coupled to alkanolamine addition, which mainly affects to sulphate dissolution and C_4AF and C_3A hydrations. Because SCMs are usually rich in aluminates with pozzolanic activities that can be accelerated [44], this feature could be particularly important for activating low-CO_2 cements based on high Portland clinker replacement fractions. The synergistic effect, measured here, has been independently reported for one blended cement prepared by a PC and a fly ash with high alumina content, 35.6 wt%, [27]. However, more research is needed to confirm and extend these findings to the large family of sustainable low-CO_2 cements.

5. Conclusions

Two main conclusions can be drawn from this work:

Firstly, synergy between C-S-H seeding and alkanolamines is proved as the dissolutions of calcium sulphate and aluminate phases are further enhanced when compared to single admixture dosage.

Secondly, C-S-H seeding accelerates the Portland and Belite cement hydration at early ages mainly by boosting calcium sulphate(s) and calcium aluminate(s) availabilities. In the studied experimental conditions, and at early hydration ages, alite and belite phase reactivities are not significantly enhanced.

CRediT authorship contribution statement

Alejandro Morales-Cantero: Methodology, Investigation, Data curation, Writing – original draft, Writing – review & editing. **Ana Cuesta:** Investigation, Writing – review & editing. **Angeles G. De la Torre:** Investigation, Writing – review & editing. **Isabel Santacruz:** Investigation, Writing – review & editing. **Oliver Mazanec:**

Conceptualization, Investigation, Writing – review & editing. **Pere Borralleras:** Investigation, Writing – review & editing. **Kai Steffen Weldert:** Investigation, Writing – review & editing. **Daniela Gastaldi:** Investigation, Writing – review & editing. **Fulvio Canonico:** Conceptualization, Investigation, Writing – review & editing. **Miguel A.G. Aranda:** Supervision, Conceptualization, Investigation, Writing – original draft, Writing – review & editing.

Declaration of competing interest

It is stated that Master Builders Solutions has a research contract with the research group of University of Malaga concerning the activation of low-CO_2 cements by admixtures. It is also stated that Buzzi Unicem has a research contract with the group of University of Malaga concerning hydration studies of belite cements. In any case, the data obtained, analysed and reported here are based on the best scientific practices. Furthermore, the companies have not issued any guideline on how to analyse neither report the data. The raw research data underlining this work have been openly deposited, see next.

Acknowledgement

This research has been partly supported by two research grants PID2020-114650RB-I00 (from Spanish Government) and P18-RT-720 (from Junta de Andalucía, Spain), which are co-funded by ERDF. ALBA synchrotron is thanked for granting beamtime at BL04-MSPD beamline. We also thank the assistance of Dr. Oriol Vallcorba during the synchrotron experiment and thorough discussion of this work with Peter Schwesig (Master Builders Solutions). Funding for open access charge: Universidad de Malaga/CBUA.

Data availability

Raw data from the following techniques, isothermal calorimetry, rheology, thermogravimetric data, laboratory X-ray powder diffraction patterns, and synchrotron powder diffraction may be openly accessed on Zenodo at https://doi.org/10.5281/zenodo.5513610, and used under the Creative Commons Attribution license. Full details of the different datasets are given in Supplementary information.

Appendix A. Supplementary data

Supplementary data to this article can be found online at https://doi.org/10.1016/j.cemconres.2022.106946.

References

[1] Global energy and CO2 emissions in 2020 – Global Energy Review 2020 – Analysis - IEA (n.d.), https://www.iea.org/reports/global-energy-review-2020/global-energy-and-co2-emissions-in-2020. (Accessed 26 January 2021).
[2] H.F.W. Taylor, Cement Chemistry, 2nd ed., Thomas Telford Pub, London, UK, 1997.
[3] Cement Sustainability Initiativecollab <collab>W.B.C. for Sustainable Development, Cement Industry Energy And CO2 Performance "Getting the Numbers Right,", Cem. Sustain. Initiat., 2009.
[4] G. Habert, S.A. Miller, V.M. John, J.L. Provis, A. Favier, A. Horvath, K.L. Scrivener, Environmental impacts and decarbonization strategies in the cement and concrete industries, Nat. Rev. Earth Environ. 1 (2020) 559–573, https://doi.org/10.1038/s43017-020-0093-3.
[5] S.A. Miller, F.C. Moore, Climate and health damages from global concrete production, Nat. Clim. Chang. 10 (2020) 439–443, https://doi.org/10.1038/s41558-020-0733-0.
[6] S.A. Miller, R.J. Myers, Environmental impacts of alternative cement binders, Environ. Sci. Technol. 54 (2020) 677–686, https://doi.org/10.1021/acs.est.9b05550.
[7] C. Shi, B. Qu, J.L. Provis, Recent progress in low-carbon binders, Cem. Concr. Res. 122 (2019) 227–250, https://doi.org/10.1016/J.CEMCONRES.2019.05.009.
[8] U.N. Environment, K.L. Scrivener, V.M. John, E. Gartner, Eco-efficient cements: potential, economically viable solutions for a low-CO2, cement-based materials industry, Cem. Concr. Res. 114 (2018) 2–26, https://doi.org/10.1016/j.cemconres.2018.03.015.
[9] L. Barcelo, J. Kline, G. Walenta, E. Gartner, Cement and carbon emissions, Mater. Struct. 47 (2014) 1055–1065, https://doi.org/10.1617/s11527-013-0114-5.
[10] S.J. Davis, N.S. Lewis, M. Shaner, S. Aggarwal, D. Arent, I.L. Azevedo, S.M. Benson, T. Bradley, J. Brouwer, Y.M. Chiang, C.T.M. Clack, A. Cohen, S. Doig, J. Edmonds, P. Fennell, C.B. Field, B. Hannegan, B.M. Hodge, M.I. Hoffert, E. Ingersoll, P. Jaramillo, K.S. Lackner, K.J. Mach, M. Mastrandrea, J. Ogden, P.F. Peterson, D. L. Sanchez, D. Sperling, J. Stagner, J.E. Trancik, C.J. Yang, K. Caldeira, Net-zero emissions energy systems, Science (80-.) 360 (2018), https://doi.org/10.1126/science.aas9793.
[11] P.J.M. Monteiro, S.A. Miller, A. Horvath, Towards sustainable concrete, Nat. Mater. 16 (2017) 698–699.
[12] M. Alexander, H. Beushausen, Durability, service life prediction, and modelling for reinforced concrete structures – review and critique, Cem. Concr. Res. 122 (2019) 17–29, https://doi.org/10.1016/J.CEMCONRES.2019.04.018.
[13] M.C.G. Juenger, R. Siddique, Recent advances in understanding the role of supplementary cementitious materials in concrete, Cem. Concr. Res. 78 (2015) 71–80, https://doi.org/10.1016/j.cemconres.2015.03.018.
[14] M.C.G. Juenger, R. Snellings, S.A. Bernal, Supplementary cementitious materials: new sources, characterization, and performance insights, Cem. Concr. Res. 122 (2019) 257–273, https://doi.org/10.1016/J.CEMCONRES.2019.05.008.
[15] V.M. John, B.L. Damineli, M. Quattrone, R.G. Pileggi, Fillers in cementitious materials — experience, recent advances and future potential, Cem. Concr. Res. 114 (2018) 65–78, https://doi.org/10.1016/J.CEMCONRES.2017.09.013.
[16] A. Cuesta, A. Ayuela, M.A.G. Aranda, Belite cements and their activation, Cem. Concr. Res. 140 (2021), 106319, https://doi.org/10.1016/j.cemconres.2020.106319.
[17] R.J. Flatt, N. Roussel, C.R. Cheeseman, Concrete: an eco material that needs to be improved, J. Eur. Ceram. Soc. 32 (2012) 2787–2798, https://doi.org/10.1016/J.JEURCERAMSOC.2011.11.012.
[18] F. Boscaro, M. Palacios, R.J. Flatt, Formulation of low clinker blended cements and concrete with enhanced fresh and hardened properties, Cem. Concr. Res. 150 (2021), 106605, https://doi.org/10.1016/J.CEMCONRES.2021.106605.
[19] M. Sharma, S. Bishnoi, F. Martirena, K. Scrivener, Limestone calcined clay cement and concrete: a state-of-the-art review, Cem. Concr. Res. 149 (2021), 106564, https://doi.org/10.1016/j.cemconres.2021.106564.
[20] J.J. Thomas, H.M. Jennings, J.J. Chen, Influence of nucleation seeding on the hydration mechanisms of tricalcium silicate and cement, J. Phys. Chem. C 113 (2009) 4327–4334, https://doi.org/10.1021/jp809811w.
[21] R. Alizadeh, L. Raki, J.M. Makar, J.J. Beaudoin, I. Moudrakovski, Hydration of tricalcium silicate in the presence of synthetic calcium-silicate-hydrate, J. Mater. Chem. 19 (2009) 7937–7946, https://doi.org/10.1039/b910216g.
[22] P. Bost, M. Regnier, M. Horgnies, Comparison of the accelerating effect of various additions on the early hydration of Portland cement, Constr. Build. Mater. 113 (2016) 290–296, https://doi.org/10.1016/j.conbuildmat.2016.03.052.
[23] E. Gartner, D. Myers, Influence of tertiary alkanolamines on Portland cement hydration, J. Am. Ceram. Soc. 76 (1993) 1521–1530, https://doi.org/10.1111/j.1151-2916.1993.tb03934.x.
[24] Z. Xu, W. Li, J. Sun, Y. Hu, K. Xu, S. Ma, X. Shen, Research on cement hydration and hardening with different alkanolamines, Constr. Build. Mater. 141 (2017) 296–306, https://doi.org/10.1016/j.conbuildmat.2017.03.010.
[25] F. Zunino, K.L. Scrivener, Assessing the effect of alkanolamine grinding aids in limestone calcined clay cements hydration, Constr. Build. Mater. (2021), https://doi.org/10.1016/j.conbuildmat.2020.121293. In press.
[26] T. Hirsch, Z. Lu, D. Stephan, Effect of different sulphate carriers on Portland cement hydration in the presence of triethanolamine, Constr. Build. Mater. 294 (2021), 123528, https://doi.org/10.1016/j.conbuildmat.2021.123528.
[27] J. He, G. Long, K. Ma, Y. Xie, Z. Cheng, Improvement of the hydration of a fly ash-cement system by the synergic action of triethanolamine and C-S-H seeding, ACS Sustain. Chem. Eng. 9 (2021) 2804–2815, https://doi.org/10.1021/acssuschemeng.0c08618.
[28] E. John, T. Matschei, D. Stephan, Nucleation seeding with calcium silicate hydrate – a review, Cem. Concr. Res. 113 (2018) 74–85, https://doi.org/10.1016/J.CEMCONRES.2018.07.003.
[29] G. Artioli, G. Ferrari, M.C. Dalconi, L. Valentini, Nanoseeds as modifiers of the cement hydration kinetics, in: M. Shahir Liew, P. Nguyen-Tri, T.A. Nguyen, S. Kakooei (Eds.), Smart Nanoconcretes Cem. Mater. Prop. Model. Appl, Elsevier, 2020, pp. 257–269, https://doi.org/10.1016/B978-0-12-817854-6.00010-6.
[30] L. Nicoleau, A. Nonat, A new view on the kinetics of tricalcium silicate hydration, Cem. Concr. Res. 86 (2016) 1–11, https://doi.org/10.1016/J.CEMCONRES.2016.04.009.
[31] E. Gartner, Discussion of the paper "A new view on the kinetics of tricalcium silicate hydration," by Nicoleau, L. and Nonat, A. Cem.Concr. Res. 86 (2016) 1–11, Cem. Concr. Res. 104 (2018) 114–117.
[32] L. Nicoleau, A. Nonat, D. Daval, Rate-limiting reaction of C3S hydration - a reply to the discussion "A new view on the kinetics of tricalcium silicate hydration" by E. Gartner, Cem. Concr. Res. 104 (2018) 118–122.
[33] G. Artioli, L. Valentini, M.C. Dalconi, M. Parisatto, M. Voltolini, V. Russo, G. Ferrari, Imaging of nano-seeded nucleation in cement pastes by X-ray diffraction tomography, Int. J. Mater. Res. 105 (2014) 628–631, https://doi.org/10.3139/146.111049.
[34] D. Zhao, R. Khoshnazar, Hydration and microstructural development of calcined clay cement paste in the presence of calcium-silicate-hydrate (C–S–H) seed, Cem. Concr. Compos. 122 (2021), 104162, https://doi.org/10.1016/j.cemconcomp.2021.104162.

[35] L. Valentini, G. Ferrari, V. Russo, M. Štefančič, V.Z. Serjun, G. Artioli, Use of nanocomposites as permeability reducing admixtures, J. Am. Ceram. Soc. 101 (2018) 4275–4284, https://doi.org/10.1111/JACE.15548.
[36] G. Land, D. Stephan, The effect of synthesis conditions on the efficiency of C-S-H seeds to accelerate cement hydration, Cem. Concr. Compos. 87 (2018) 73–78, https://doi.org/10.1016/j.cemconcomp.2017.12.006.
[37] L. Nicoleau, The acceleration of cement hydration by seeding: influence of the cement mineralogy, ZKG Int. (2013) 40–49.
[38] H.C. Pedrosa, O.M. Reales, V.D. Reis, M. das D. Paiva, E.M.R. Fairbairn, Hydration of Portland cement accelerated by C-S-H seeds at different temperatures, Cem. Concr. Res. 129 (2020), 105978, https://doi.org/10.1016/j.cemconres.2020.105978.
[39] M. Boháč, T. Staněk, A. Zezulová, A. Rybová, D. Kubátová, R. Novotný, Early hydration of activated belite-rich cement, Adv. Mater. Res. 1151 (2019) 23–27, https://doi.org/10.4028/www.scientific.net/AMR.1151.23.
[40] V. Kanchanason, J. Plank, Effectiveness of a calcium silicate hydrate – polycarboxylate ether (C-S-H–PCE) nanocomposite on early strength development of fly ash cement, Constr. Build. Mater. 169 (2018) 20–27, https://doi.org/10.1016/J.CONBUILDMAT.2018.01.053.
[41] B. Szostak, G.L. Golewski, Effect of nano admixture of CSH on selected strength parameters of concrete including fly ash, IOP Conf. Ser. Mater. Sci. Eng. 416 (2018), 012105, https://doi.org/10.1088/1757-899X/416/1/012105.
[42] C. Ouellet-Plamondon, S. Scherb, M. Köberl, K.C. Thienel, Acceleration of cement blended with calcined clays, Constr. Build. Mater. 245 (2020), 118439, https://doi.org/10.1016/J.CONBUILDMAT.2020.118439.
[43] F. Zou, C. Hu, F. Wang, Y. Ruan, S. Hu, Enhancement of early-age strength of the high content fly ash blended cement paste by sodium sulfate and C-S–H seeds towards a greener binder, J. Clean. Prod. 244 (2020), 118566, https://doi.org/10.1016/J.JCLEPRO.2019.118566.
[44] F. Zou, K. Shen, C. Hu, F. Wang, L. Yang, S. Hu, Effect of sodium sulfate and C-S–H seeds on the reaction of fly ash with different amorphous alumina contents, ACS Sustain. Chem. Eng. 8 (2020) 1659–1670, https://doi.org/10.1021/ACSSUSCHEMENG.9B06779.
[45] B. Szostak, G.L. Golewski, Improvement of strength parameters of cement matrix with the addition of siliceous fly ash by using nanometric C-S-H seeds, Energies 13 (2020) 6734, https://doi.org/10.3390/EN13246734.
[46] F. Canonico, Special binders as an alternative to Portland cement, in: 20th Int. Conf. Build. Mater, 2015, pp. 410–422. Weimar.
[47] A.G. De la Torre, S. Bruque, M.A.G. Aranda, Rietveld quantitative amorphous content analysis, J. Appl. Crystallogr. 34 (2001) 196–202, https://doi.org/10.1107/S0021889801002485.
[48] A.C. Larson, R.B. Von Dreele, in: General Structure Analysis System (GSAS) 748, Los Alamos Natl. Lab. Rep. LAUR, 2004, pp. 86–748.
[49] F. Fauth, I. Peral, C. Popescu, M. Knapp, The New Material Science Powder Diffraction Beamline at ALBA Synchrotron, Cambridge University Press, 2013, https://doi.org/10.1017/S0885715613000900.
[50] B.H. Toby, R.B.Von Dreele, in: IUCr, GSAS-II: the genesis of a modern open-source all purpose crystallography software package, 2013, pp. 544–549, https://doi.org/10.1107/S0021889813003531.
[51] A.G.De la Torre, I. Santacruz, A. Cuesta, L. León-Reina, M.A.G. Aranda, Diffraction and crystallography applied to anhydrous cements, in: H. Pöllmann (Ed.), Cem. Mater, De Gruyter, 2017, pp. 3–29.
[52] M.A.G. Aranda, A. Cuesta, A.G.De la Torre, I. Santacruz, L. León-Reina, Diffraction and crystallography applied to hydrating cements, in: H. Pöllmann (Ed.), Cem. Mater. Compos. Prop. Appl, De Gruyter, Berlin, Boston, Germany, 2017, pp. 31–60, https://doi.org/10.1515/9783110473728-003.
[53] A. Cuesta, J.D. Zea-Garcia, D. Londono-Zuluaga, A.G. De la Torre, I. Santacruz, O. Vallcorba, M. Dapiaggi, S.G. Sanfélix, M.A.G. Aranda, Multiscale understanding of tricalcium silicate hydration reactions, Sci. Rep. 8 (2018) 8544, https://doi.org/10.1038/s41598-018-26943-y.
[54] A. Morales-Cantero, A.G. De la Torre, A. Cuesta, E. Fraga-Lopez, S. Shirani, M.A. G. Aranda, Belite hydration at high temperature and pressure by in situ synchrotron powder diffraction, Constr. Build. Mater. 262 (2020), 120825, https://doi.org/10.1016/j.conbuildmat.2020.120825.
[55] S. Shirani, A. Cuesta, A. Morales-Cantero, A.G. De la Torre, M.P. Olbinado, M.A. G. Aranda, Influence of curing temperature on belite cement hydration: a comparative study with Portland cement, Cem. Concr. Res. 147 (2021), 106499, https://doi.org/10.1016/j.cemconres.2021.106499.
[56] L. Nicoleau G. Albrecht K. Lorenz E. Jetzlsperger D. Fridrich T. Wohlhaupter R. Dorfner H. Leitner M. Vierle D. Schmitt M. Braeu C. Hesse S.M. Pancera S. Zuern M. Kutschera, Plasticizer-containing Hardening Accelerator Composition, US8653186B2, 2014. https://patents.google.com/patent/US8653186B2/en.
[57] A. Alzaza, K. Ohenoja, I. Langås, B. Arntsen, M. Poikelispää, M. Illikainen, Low-temperature (−10 oC) curing of Portland cement paste – synergetic effects of chloride-free antifreeze admixture, C-S–H seeds, and room-temperature pre-curing, Cem. Concr. Compos. 125 (2022), 104319, https://doi.org/10.1016/j.cemconcomp.2021.104319.
[58] K.L. Scrivener, P. Juilland, P.J.M. Monteiro, Advances in understanding hydration of Portland cement, Cem. Concr. Res. 78 (2015) 38–56, https://doi.org/10.1016/J.CEMCONRES.2015.05.025.
[59] K.L. Scrivener, A. Ouzia, P. Juilland, A. Kunhi Mohamed, Advances in understanding cement hydration mechanisms, Cem. Concr. Res. 124 (2019), 105823, https://doi.org/10.1016/j.cemconres.2019.105823.
[60] G. Trtnik, M. Gams, Recent advances of ultrasonic testing of cement based materials at early ages, Ultrasonics 54 (2014) 66–75, https://doi.org/10.1016/j.ultras.2013.07.010.
[61] B.H.U. Tekle, L. Hertwig, K. Holschemacher, Setting time and strength monitoring of alkali-activated cement mixtures by ultrasonic testing, Materials (Basel) 14 (2021) 1889, https://doi.org/10.3390/ma14081889.
[62] G. Hong, S. Oh, S. Choi, W.J. Chin, Y.J. Kim, C. Song, Correlation between the compressive strength and ultrasonic pulse velocity of cement mortars blended with silica fume: an analysis of microstructure and hydration kinetics, Materials 14 (2021) 2476, https://doi.org/10.3390/MA14102476.
[63] B. Lothenbach, P. Durdzinski, K.De Weerdt, Thermogravimetric analysis, in: B.L. K. Scrivener, R. Snellings (Eds.), A Pract. Guid. to Microstruct. Anal. Cem. Mater, CRC Press, U.S.A, 2016, pp. 177–211.
[64] T. Dorn, O. Blask, D. Stephan, Acceleration of cement hydration – a review of the working mechanisms, effects on setting time, and compressive strength development of accelerating admixtures, Constr. Build. Mater. 323 (2022), 126554, https://doi.org/10.1016/j.conbuildmat.2022.126554.
[65] V.M. John, M. Quattrone, P.C.R.A. Abrão, F.A. Cardoso, Rethinking cement standards: opportunities for a better future, Cem. Concr. Res. 124 (2019), 105832, https://doi.org/10.1016/J.CEMCONRES.2019.105832.
[66] M.A.G. Aranda, A.G. De la Torre, L. Leon-Reina, Rietveld quantitative phase analysis of OPC clinkers, cements and hydration products, Rev. Mineral. Geochem. 74 (2012) 169–209, https://doi.org/10.2138/rmg.2012.74.5.
[67] A. Cuesta, A.G. De la Torre, I. Santacruz, A. Diaz, P. Trtik, M. Holler, B. Lothenbach, M.A.G. Aranda, Quantitative disentanglement of nanocrystalline phases in cement pastes by synchrotron ptychographic X-ray tomography, IUCrJ 6 (2019) 473–491, https://doi.org/10.1107/S2052252519003774.
[68] A.J. Allen, J.J. Thomas, H.M. Jennings, Composition and density of nanoscale calcium–silicate–hydrate in cement, Nat. Mater. 6 (2007) 311–316, https://doi.org/10.1038/nmat1871.
[69] E.M.J. Bérodier, A.C.A. Muller, K.L. Scrivener, Effect of sulfate on C-S-H at early age, Cem. Concr. Res. 138 (2020), 106248, https://doi.org/10.1016/j.cemconres.2020.106248.
[70] W. Li, M. Fall, Sulphate effect on the early age strength and self-desiccation of cemented paste backfill, Constr. Build. Mater. 106 (2016) 296–304, https://doi.org/10.1016/J.CONBUILDMAT.2015.12.124.
[71] L. Nicoleau, E. Schreiner, A. Nonat, Ion-specific effects influencing the dissolution of tricalcium silicate, Cem. Concr. Res. 59 (2014) 118–138, https://doi.org/10.1016/j.cemconres.2014.02.006.
[72] E. Pustovgar, R.K. Mishra, M. Palacios, J.-B. d'Espinose de Lacaillerie, T. Matschei, A.S. Andreev, H. Heinz, R. Verel, R.J. Flatt, Influence of aluminates on the hydration kinetics of tricalcium silicate, Cem. Concr. Res. 100 (2017) 245–262, https://doi.org/10.1016/j.cemconres.2017.06.006.
[73] D. Wagner, F. Bellmann, J. Neubauer, Influence of aluminium on the hydration of triclinic C3S with addition of KOH solution, Cem. Concr. Res. 137 (2020), 106198, https://doi.org/10.1016/j.cemconres.2020.106198.
[74] T. Dorn, T. Hirsch, D. Stephan, Analyzing the early structural build-up of accelerated cement pastes, Mater. Struct. 54 (2021) 1–15, https://doi.org/10.1617/s11527-021-01662-5.
[75] P. Juilland, E. Gallucci, R. Flatt, K.L. Scrivener, Dissolution theory applied to the induction period in alite hydration, Cem. Concr. Res. 40 (2010) 831–844, https://doi.org/10.1016/J.CEMCONRES.2010.01.012.
[76] F. Zunino, K.L. Scrivener, Factors influencing the sulfate balance in pure phase C3S/C3A systems, Cem. Concr. Res. 133 (2020), https://doi.org/10.1016/j.cemconres.2020.106085.
[77] P. Suraneni, R.J. Flatt, Micro-reactors to study alite hydration, J. Am. Ceram. Soc. 98 (2015) 1634–1641, https://doi.org/10.1111/jace.13472.
[78] P. Suraneni, M. Palacios, R.J. Flatt, New insights into the hydration of slag in alkaline media using a micro-reactor approach, Cem. Concr. Res. 79 (2016) 209–216, https://doi.org/10.1016/j.cemconres.2015.09.015.

Supporting Information

C-S-H seeding activation of Portland and Belite Cements: an enlightening *in situ* synchrotron powder diffraction study

Alejandro Morales-Cantero[1], Ana Cuesta[1], Angeles G. De la Torre[1], Isabel Santacruz[1], Oliver Mazanec[2], Pere Borralleras[3], Kai Steffen Weldert[2], Daniela Gastaldi[4], Fulvio Canonico[4], Miguel A. G. Aranda[1]*

[1]*Departamento de Química Inorgánica, Cristalografía y Mineralogía, Universidad de Málaga, Málaga, 29071, Spain*

[2] *Master Builders Solutions Deutschland GmbH, Albert-Frank Str. 32, 83308 Trostberg, Germany*

[3] *Master Builders Solutions España S.L.U., Carretera de l'Hospitalet, 147-149, Edificio Viena, 1ª planta, 08940 Cornellà de Llobregat, Spain*

[4] *Research & Development, Buzzi Unicem, Via Luigi Buzzi 6, 15033 Casale Monferrato, Italy*

** email: g_aranda@uma.es*

This file contains:

Table S1. Elemental composition (wt%) for the three anhydrous cements from XRF.

Table S2. Rietveld quantitative phase analysis (wt%) for the anhydrous cements from SXRPD.

Table S3. Rietveld quantitative phase analysis (wt%) for the anhydrous cements from LXRPD.

Table S4. Quantitative data from the calorimetric traces shown in Fig. 1 of the main paper.

Table S5. CH content (wt%), free water content (wt%) and total mass loss (%) from the thermal study displayed in Fig. 3 of the main paper.

- **Characterisation of the employed natural gypsum material.**
- ***In situ* rheological study.**
- **Raw data availability and description.**
- **Calculations of phase and water contents** based on chemical reactions and the RQPA results.

Fig. S1. Synchrotron powder X-ray diffraction Rietveld plot (λ=0.62005 Å) for the anhydrous cements: (a) PC-42.5, (b) BC-Buz and (c) BC-n.a.

Fig. S2. Particle size distribution, surface area BET, air permeability and density for PC-42.5 (black), BC-Buz (blue) and BC-n.a. (red) cements.

Fig S3. Laboratory powder X-ray diffraction Rietveld plots, MoKα_1, for hydrated pastes at 28d (a) PC-42.5-Ref, (b) BC-Buz-Ref and (c) BC-n.a.-Ref.

Fig S4. Laboratory powder X-ray diffraction Rietveld plot, MoKα_1, for hydrated pastes at 28d (a) PC-42.5-XS130, (b) BC-Buz-XS130 and (c) BC-n.a.-XS130.

Fig S5. Synchrotron X-ray powder diffraction raw patterns (λ=0.62005 Å) for the PC-42.5-Ref (left panels) and PC-42.5-XS130 (right panels). The 2θ windows have been chosen for better qualitative visualisation of the main phase changes.

Fig S6. Synchrotron X-ray powder diffraction raw patterns (λ=0.62005 Å) for the BC-Buz-Ref (left panels) and BC-Buz-XS130 (right panels). The 2θ windows have been chosen for better qualitative visualisation of the main phase changes.

Fig S7. Synchrotron X-ray powder diffraction raw patterns (λ=0.62005 Å) for the BC-n.a.-Ref (left panels) and BC-n.a.-XS130 (right panels). The 2θ windows have been chosen for better qualitative visualisation of the main phase changes.

Table S1. Elemental composition (wt%) for the three anhydrous cements from XRF.

	CaO	SiO_2	SO_3	Al_2O_3	Fe_2O_3	MgO	K_2O	Na_2O	Others	LoI
PC-42.5	62.9	19.7	3.4	5.0	3.4	1.5	1.1	0.3	0.3	2.7
BC-Buz	59.3	21.4	4.8	4.3	2.8	2.7	0.9	0.2	0.9	2.9
BC-n.a.	60.1	24.4	2.8	2.9	4.8	1.2	0.5	0.1	1.3	2.0

Table S2. Rietveld quantitative phase analysis (wt%) for the anhydrous cements from SXRPD.

	C_3S*	$C_2S^{\$}$	C_4AF	$C_3A^{\#}$	$C_4A_3\bar{S}$	MgO	$C\bar{C}$	$C\bar{S}H_2$	$C\bar{S}H_{0.5}$	$C\bar{S}$	ACn
PC-42.5	50.0	7.5	9.6	6.8	-	-	3.6	1.0	2.0	-	19.5
BC-Buz	23.0	46.9	10.4	3.4	1.9	1.8	3.4	-	-	2.1	7.1
BC-n.a.	29.2	47.4	14.4	-	-	-	-	2.8	-	-	6.2

*PC-42.5: C_3S-M_3; BC-Buz: 2.9wt% C_3S-M_3 and 21.9wt% C_3S-M_1; BC-n.a.: 1.8wt% C_3S-M_3 and 26.8wt% C_3S-M_1
$^{\$}$PC-42.5: β-$C_2S$; BC-Buz: 45.4wt% β-$C_2S$ and 1.5wt% α-C_2S; BC-n.a.: β-C_2S
$^{\#}$PC-42.5: o-C_3A; BC-Buz: c-C_3A

Table S3. Rietveld quantitative phase analysis (wt%) for the anhydrous cements from LXRPD.

	C_3S*	β-C_2S	C_4AF	$C_3A^{\#}$	$C_4A_3\bar{S}$	MgO	$C\bar{C}$	$C\bar{S}H_2$	$C\bar{S}H_{0.5}$	$C\bar{S}$	ACn
PC-42.5	48.3	9.0	9.1	4.0	-	-	3.0	0.9	1.0	-	24.7
BC-Buz	24.8	44.1	10.1	2.0	1.9	1.4	1.3	-	-	1.6	12.8
BC-n.a.	28.6	48.0	15.2	-	-	-	-	2.0	-	-	6.2

*PC-42.5: C_3S-M_3; BC-Buz: 2.9wt% C_3S-M_3 and 21.9wt% C_3S-M_1; BC-n.a.: 1.8wt% C_3S-M_3 and 26.8wt% C_3S-M_1
$^{\#}$PC-42.5: o-C_3A; BC-Buz: c-C_3A

Table S4.
Quantitative data from the calorimetric traces shown in Fig. 1 of the main paper.

Sample	End of IP[#] (h)	Heat at 2d (J/g)	Heat at 7d (J/g)
PC-42.5-Ref	2.6	225.3	310.0
PC-42.5-XS100	1.9	239.2	307.7
PC-42.5-XS130	2.1	230.8	299.3
PC-42.5-TIPA	2.6	231.8	332.0
BC-Buz-Ref	4.3	163.1	209.7
BC-Buz-XS100	4.2	157.0	206.2
BC-Buz-XS130	4.8	171.8	227.0
BC-Buz-TIPA	4.4	170.6	238.0
BC-n.a.-Ref	10.1	146.3	193.9
BC-n.a.-XS100	6.8	151.7	199.3
BC-n.a.-XS130	5.7	147.5	223.4
BC-n.a.-TIPA	10.1	152.2	236.5

End of the induction period (IP) calculated as shown in Fig. 1a.

Table S5.
CH content (wt%), free water content (wt%) and total mass loss (%) from the thermal study displayed in Fig. 3 of the main paper.

Sample	2 days			7 days			28 days		
	CH content	FW content	Total loss	CH content	FW content	Total loss	CH content	FW content	Total loss
PC-42.5-Ref	7.5	23.3	16.9	9.4	21.4	19.5	10.8	18.1	23.0
PC-42.5-XS130	6.5	22.6	18.1	8.2	19.4	21.7	9.3	17.3	24.2
PC-42.5-TIPA	7.1	23.7	17.0	9.2	19.7	21.7	10.8	17.6	24.2
BC-Buz-Ref	3.2	24.2	15.6	3.7	22.1	15.6	4.0	20.1	21.1
BC-Buz-XS130	2.4	22.9	17.4	2.7	21.0	17.4	3.9	18.0	23.3
BC-Buz-TIPA	3.2	23.6	16.4	3.2	22.4	16.4	3.9	18.5	22.8
BC-n.a.-Ref	4.1	26.6	11.6	5.4	24.3	14.7	5.8	20.4	19.4
BC-n.a.-XS130	3.7	26.2	12.5	4.4	24.1	15.6	5.1	19.9	21.9
BC-n.a.-TIPA	4.6	25.9	12.5	3.6	25.5	13.1	5.1	21.6	18.7

♦ **Characterisation of the employed natural gypsum material.**

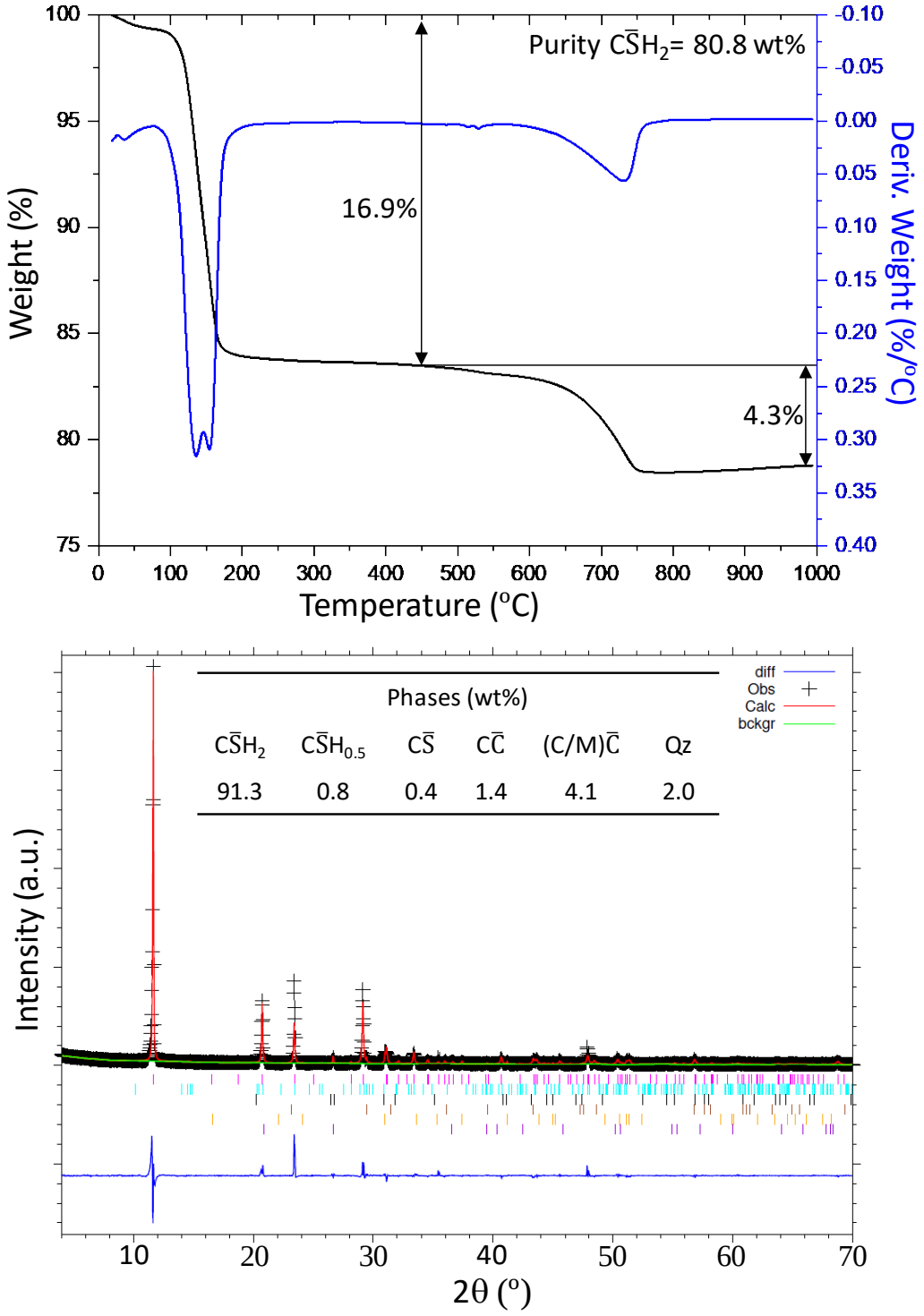

Analysis of employed gypsum material. DTA-TGA to determine the overall gypsum content from the weight loss (top), and Cu-$K_{\alpha 1}$ laboratory powder X-ray diffraction Rietveld plot (λ=1.5406 Å) to determine the crystalline phase contents (bottom).

♦ ***In situ* rheological study.** The rheological behaviour of BC-Buz mortars, prepared without and with admixtures, was studied to unravel if the higher mechanical strengths of the latter were related to a lower viscosity and hence better homogeneity of the mortars, or mainly to the hydration activation. The figure below shows the flow curves of BC-Buz-Ref, BC-Buz-XS100 and BC-Buz-XS130 mortars measured after 8 min since water and powder were mixed; that corresponds to the time needed to prepare mortar prisms. No important differences in the rheological behaviour were observed, where slightly lower values of torque, which is related to viscosity, for BC-Buz-Ref mortar were obtained. Thus, the higher mechanical strengths of mortars for BC-Buz-XS130 are mainly due to the activated hydration.

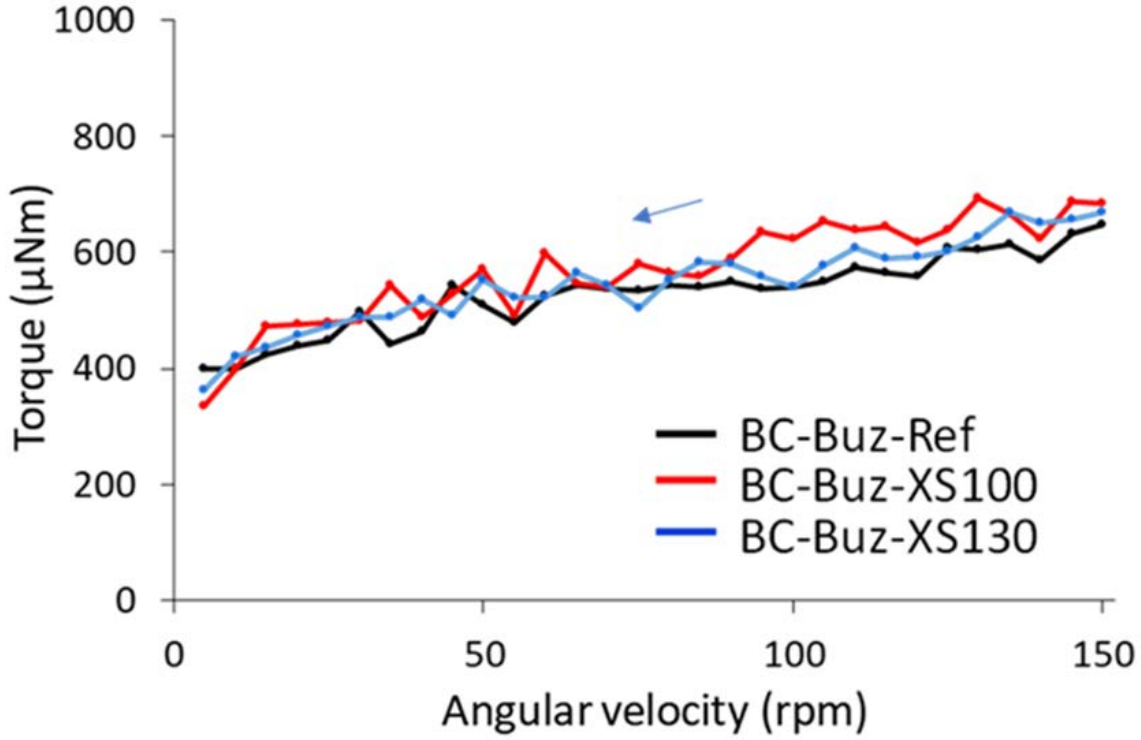

Torque vs. angular velocity of BC-Buz mortars prepared without and with admixtures at 8 min of hydration.

♦ **Raw data availability and description.**

The following raw data has been freely and openly deposited in text file or excel format: calorimetry, rheology, thermal analysis (TA), laboratory X-ray powder diffraction (LXRPD), Synchrotron X-Ray Powder Diffraction (SXRPD) and ^{27}Al magic angle spinning nuclear magnetic resonance (^{27}Al-MAS NMR). The Thermal Analysis (TA) files can be open using the TA Universal Analysis software. Data can be accessed at: https://doi.org/10.5281/zenodo.5513610.

Calorimetry
PC-425-Ref-Serie (1 file)
PC-425-XS100-Serie (1 file)
PC-425-XS130-Serie (1 file)
PC-425-TIPA-Serie (1 file)
BC-Buz-Ref-Serie (1 file)
BC-Buz-XS100-Serie (1 file)
BC-Buz-XS130-Serie (1 file)
BC-Buz-TIPA-Serie (1 file)
BC-n.a.-Ref-Serie (1 file)
BC-n.a.-XS100-Serie (1 file)
BC-n.a.-XS130-Serie (1 file)
BC-n.a.-TIPA-Serie (1 file)

LXRPD
PC-425-Anh (1 file)
PC-425-Ref-Serie (3 files)
PC-425-XS130-Serie (3 files)
PC-425-TIPA-Serie (3 files)
BC-Buz-Anh (1 file)
BC-Buz-Ref-Serie (3 files)
BC-Buz-XS130-Serie (3 files)
BC-Buz-TIPA-Serie (3 files)
BC-n.a. –Anh (1 file)
BC-n.a.-Ref-Serie (3 files)
BC-n.a.-XS130-Serie (3 files)
BC-n.a.-TIPA-Serie (3 files)
Mineral-gypsum (1 file)

^{27}Al MAS-NMR
PC-425-Ref-Serie (2 files)
PC-425-XS130-Serie (2 files)
BC-Buz-Ref-Serie (2 files)
BC-Buz-XS130-Serie (2 files)
BC-n.a.-Ref-Serie (2 files)
BC-n.a.-XS130-Serie (2 files)

Rheology
BC-Buz-Ref-Serie (1 file)
BC-Buz-XS100-Serie (1 file)
BC-Buz-XS130-Serie (1 file)

TA
PC-425-Ref-Serie (3 files)
PC-425-XS130-Serie (3 files)
PC-425-TIPA-Serie (3 files)
BC-Buz-Ref-Serie (3 files)
BC-Buz-XS130-Serie (3 files)
BC-Buz-TIPA-Serie (3 files)
BC-n.a.-Ref-Serie (3 files)
BC-n.a.-XS130-Serie (3 files)
BC-n.a.-TIPA-Serie (3 files)
Mineral-gypsum (1 file)

SXRPD
PC-425-Anh (1 file)
PC-425-Ref-Serie (30 files)
PC-425-XS100-Serie (29 files)
PC-425-XS130-Serie (29 files)
PC-425-TIPA-Serie (20 files)
BC-Buz-Anh (1 file)
BC-Buz-Ref-Serie (20 files)
BC-Buz-XS100-Serie (19 files)
BC-Buz-XS130-Serie (29 files)
BC-Buz-TIPA-Serie (18 files)
BC-n.a.-Anh (1 file)
BC-n.a.-Ref-Serie (61 files)
BC-n.a.-XS130-Serie (61 files)

♦ ***Calculations of phase and water contents based on chemical reactions and the RQPA results.***

A post-analysis calculation was performed to estimate the amount of free water, equations (1) to (7) and the amount of amorphous C–S–H gel, equations (1) and (2). The same stoichiometry for C–S–H gel has been considered from alite and belite hydration.

$$Ca_3SiO_5 + 5.2H_2O \rightarrow 1.2Ca(OH)_2 + (CaO)_{1.8}SiO_2(H_2O)_{4.0} \quad (1)$$

$$Ca_2SiO_5 + 4.2H_2O \rightarrow 0.2Ca(OH)_2 + (CaO)_{1.8}SiO_2(H_2O)_{4.0} \quad (2)$$

$$Ca_3Al_2O_6 + 3CaSO_4 + 32H_2O \rightarrow Ca_6Al_2(SO_4)_3(OH)_{12}\cdot 26H_2O \quad (3)$$

$$Ca_4Al_6O_{12}(SO_4) + 2CaSO_4 + 38\,H_2O \rightarrow Ca_6Al_2(OH)_{12}(SO_4)_3\cdot 26H_2O + 4\,Al(OH)_3 \quad (4)$$

$$Ca_4Al_2Fe_2O_{10} + 3CaSO_4\cdot 2H_2O + 30H_2O \rightarrow Ca_6Al_2(OH)_{12}(SO_4)_3\cdot 26H_2O + Ca(OH)_2 + 2Fe(OH)_3 \quad (5)$$

$$Ca_3Al_2O_6 + 0.5CaCO_3 + 0.5Ca(OH)_2 + 11.5H_2O \rightarrow Ca_4Al_2(CO_3)_{0.5}(OH)_{13}\cdot 5.5H_2O \quad (6)$$

$$Ca_3Al_2O_6 + CaCO_3 + 11H_2O \rightarrow Ca_4Al_2(CO_3)(OH)_{12}\cdot 5H_2O \quad (7)$$

Knowing the initial free water, 33.3 wt% and considering the bounded water according the stoichiometry of reactions (1) to (7), the free water at each hydration time was calculated. The amount of C–S–H gel can be estimated by the decrease of alite and belite and, *independently*, by the quantification of portlandite. The sum of the estimated FW and C–S–H gel should be close to the ACn content obtained by the internal standard method in each time of hydration. The mismatches among the ACn value and the estimated FW and C–S–H gel calculations are considered other amorphous components (mainly ♦ AFm type, ♦ iron-siliceous hydrogarnet, and ♦ the remaining fraction of amorphous phase(s) within the unreacted clinker components).

Detailed example for one calculation. The FW (free water) content from the chemical reactions for PC-42.5-Ref at 2 days of hydration is detailed next, using the main reactions, as a representative example for the calculations reported in Tables 1-3.

I. Silicate reactions: at this hydration age, there are 12.8 wt% of C_3S left. This means 33.3 wt% – 12.8 wt% = 20.5 wt% of C_3S has reacted. According to reaction (1), 8.4 wt% of water has been consumed. The same calculation can be performed with the amount of portlandite measured at 2 days of hydration, 7.8 wt% which leads (according to reaction (1)) to a water consumption of 8.2 wt%. Consequently, the average value is taken, i.e. 8.3 wt%.

II. Aluminate reactions: there are 2.8 wt% of C_3A left. This implies that, 4.5 wt% – 2.8wt% = 1.7 wt% of C_3A has reacted. According to reaction (3), 3.0 wt% of water has been consumed. The same calculation can be performed with the amount of AFt obtained at 2 days of hydration, 6.0 wt% which leads (according to reaction (3)) to a water consumption of 2.3 wt%. Consequently, the average value taken, i.e. 2.6 wt%.

So, in this case the calculated FW content for PC-42.5-Ref at 2 days of hydration is 33.3 wt% - 8.3 wt% - 2.6 wt%=**22.4 wt%**.

The same procedure has been followed for the other samples at the studied hydration ages, by employing the chemical reactions (1) to (7), as necessary.

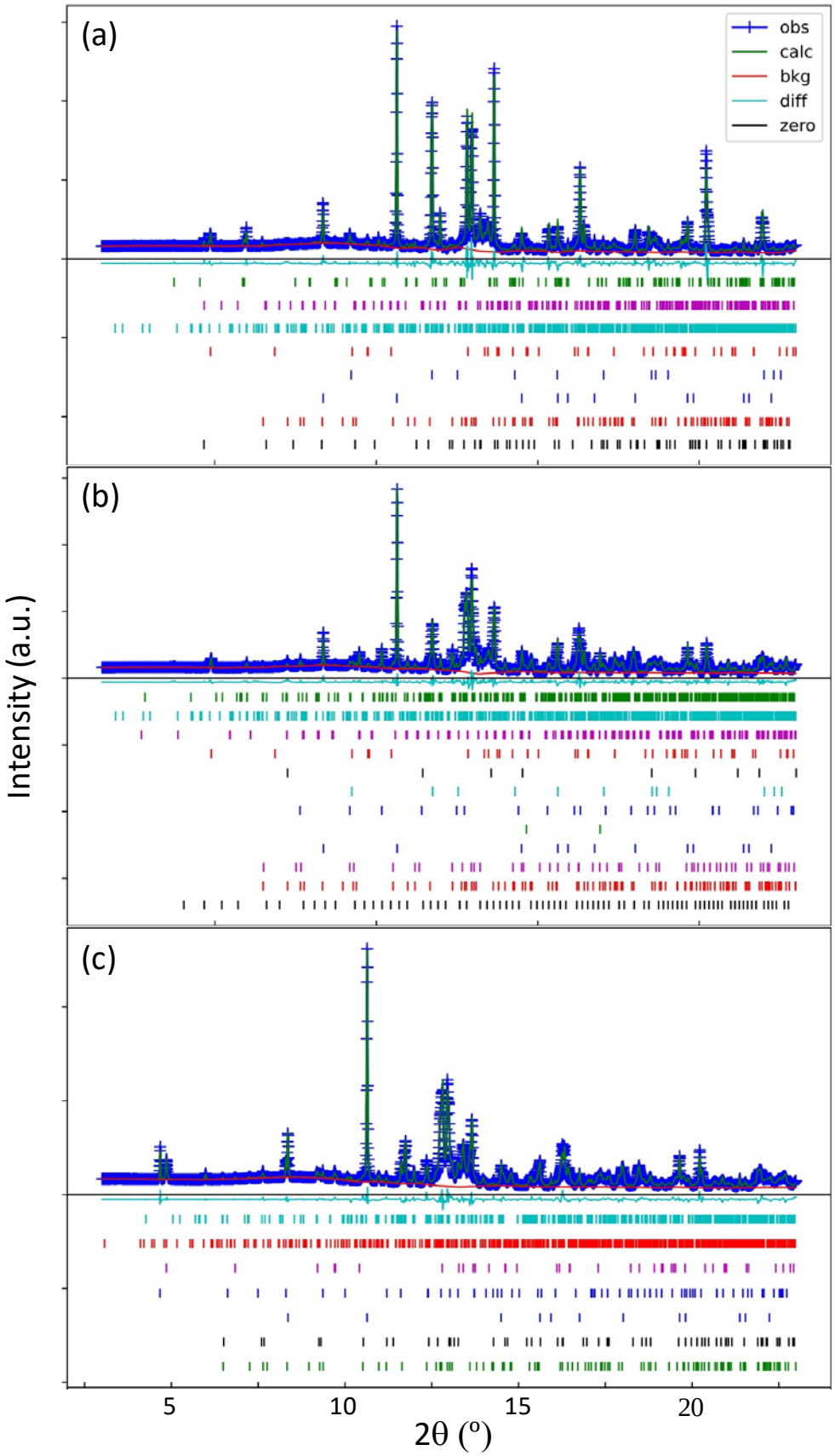

Fig. S1. Synchrotron powder X-ray diffraction Rietveld plot (λ=0.62005 Å) for the anhydrous cements: (a) PC-42.5, (b) BC-Buz and (c) BC-n.a.

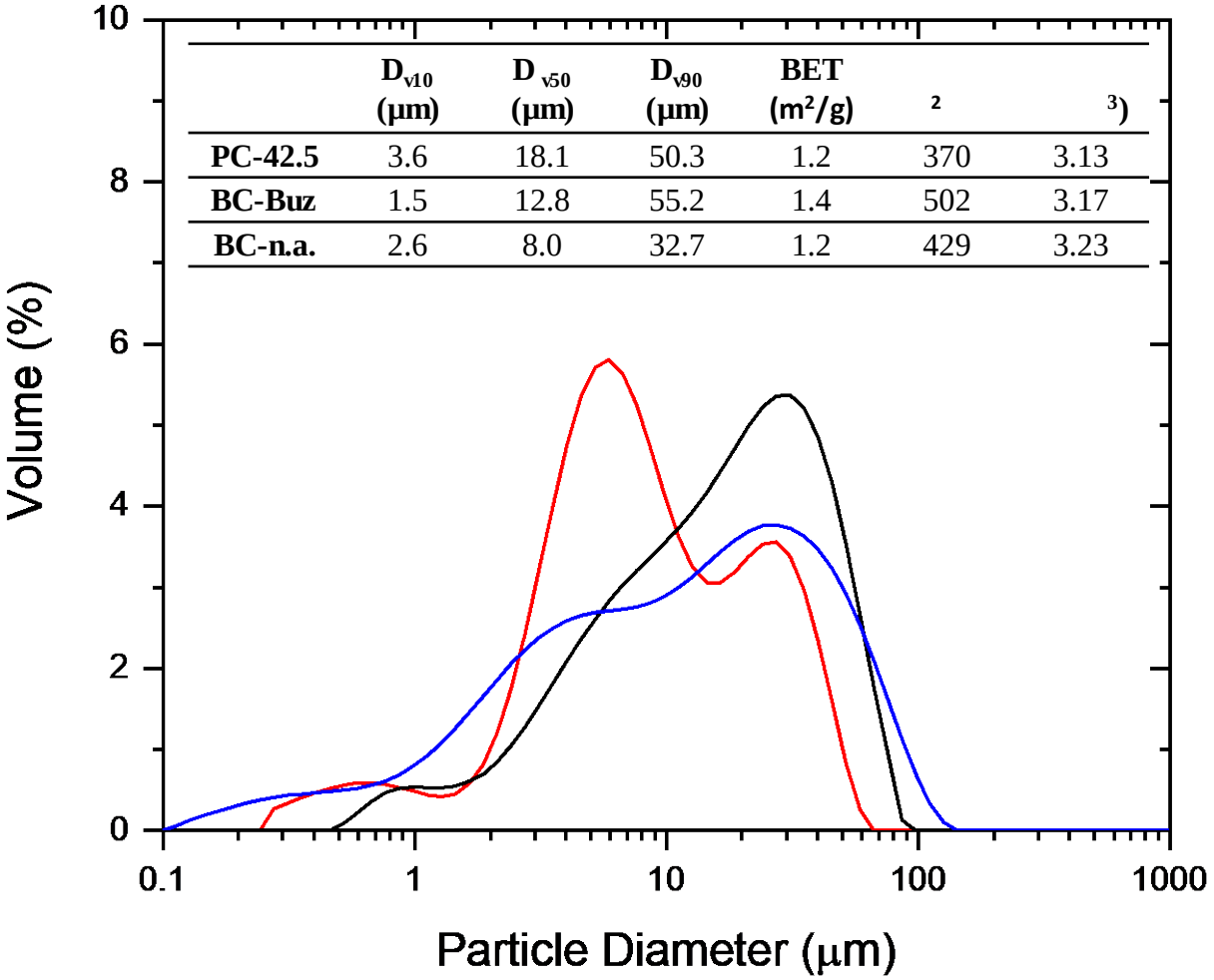

	D_{v10} (μm)	D_{v50} (μm)	D_{v90} (μm)	BET (m^2/g)	^{2}	^{3})
PC-42.5	3.6	18.1	50.3	1.2	370	3.13
BC-Buz	1.5	12.8	55.2	1.4	502	3.17
BC-n.a.	2.6	8.0	32.7	1.2	429	3.23

Fig. S2. Particle size distribution, surface area BET, air permeability and density for PC-42.5 (black), BC-Buz (blue) and BC-n.a. (red) cements.

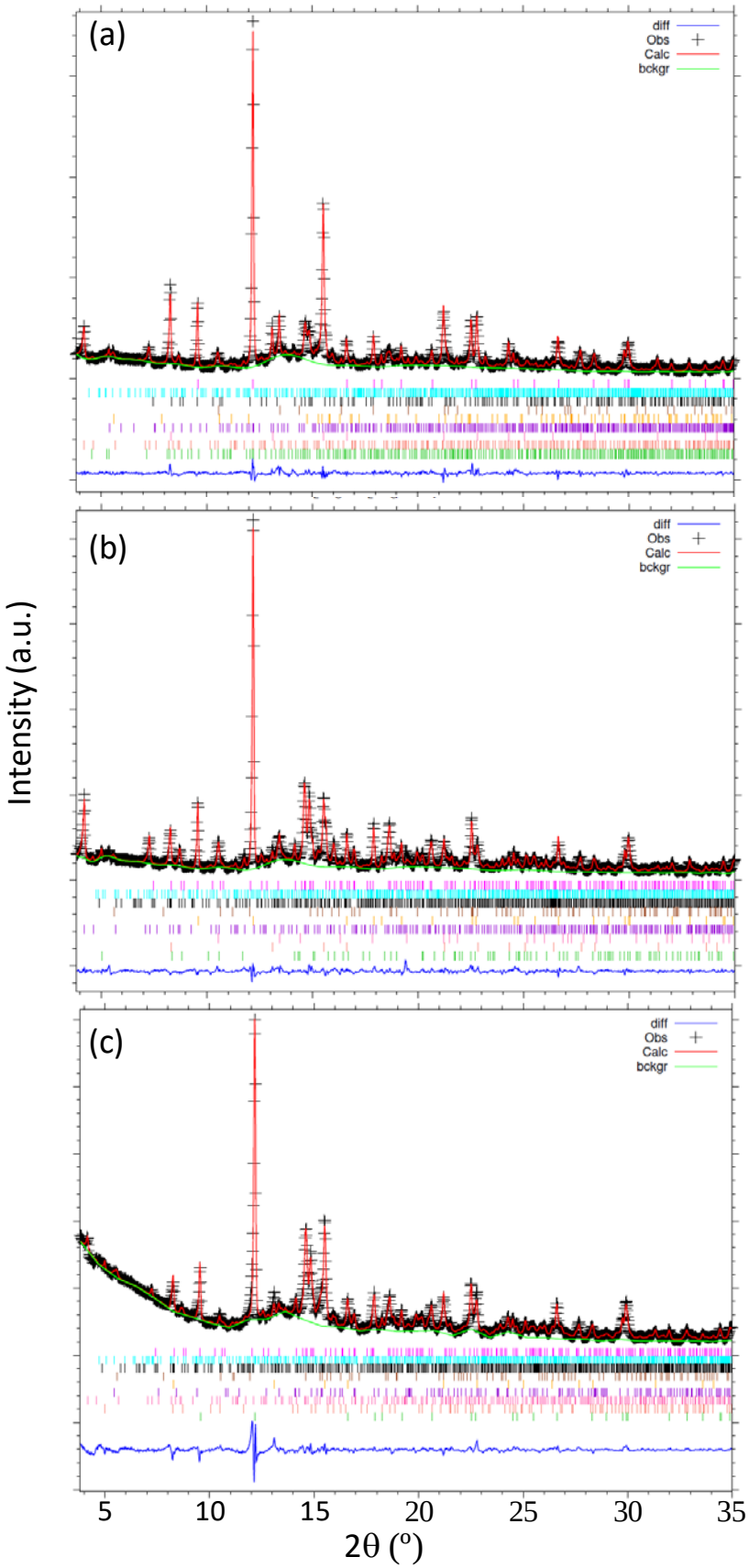

Fig S3. Laboratory powder X-ray diffraction Rietveld plots, MoKα$_1$, for hydrated pastes at 28d (a) PC-42.5-Ref, (b) BC-Buz-Ref and (c) BC-n.a.-Ref.

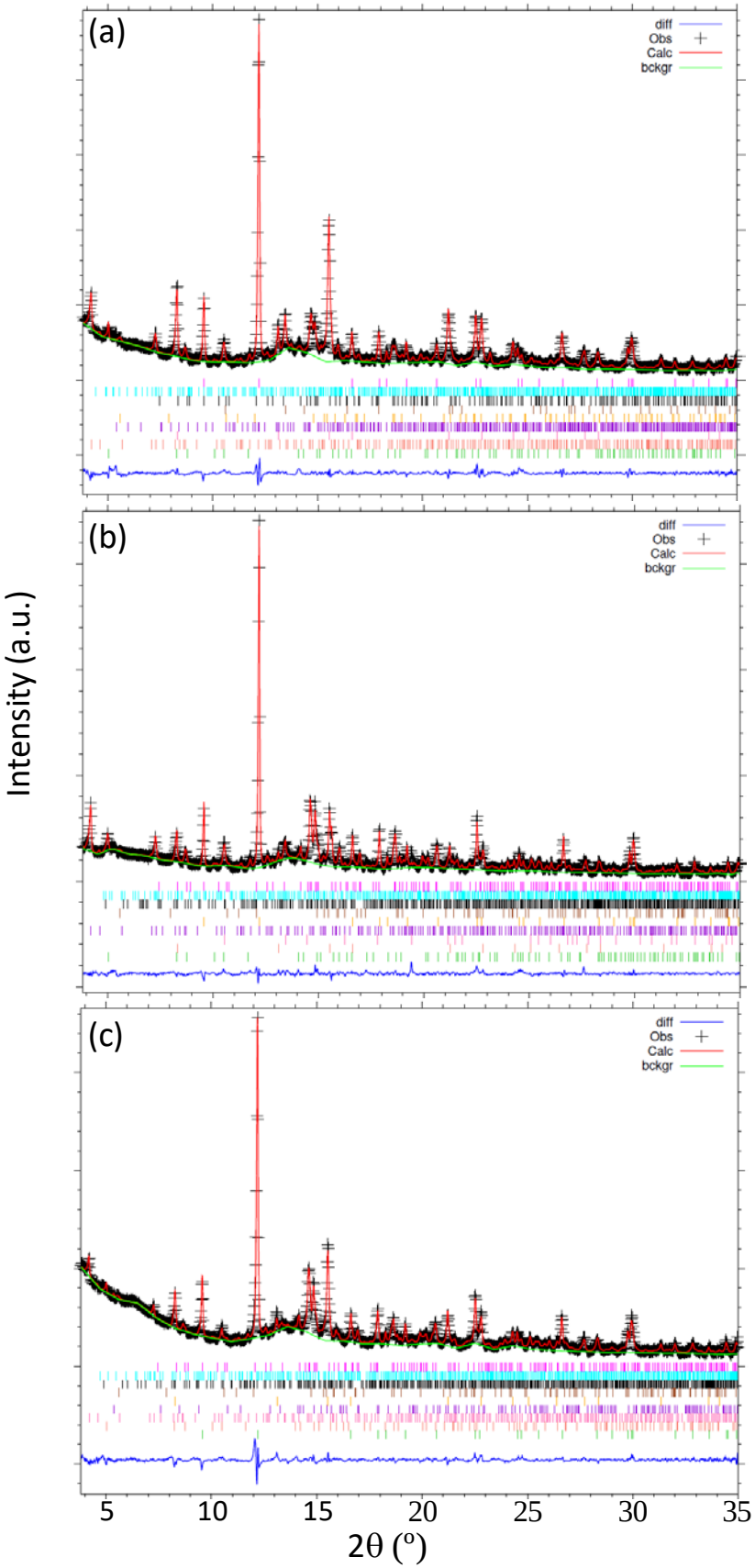

Fig S4. Laboratory powder X-ray diffraction Rietveld plot, MoKα_1, for hydrated pastes at 28d (a) PC-42.5-XS130, (b) BC-Buz-XS130 and (c) BC-n.a.-XS130.

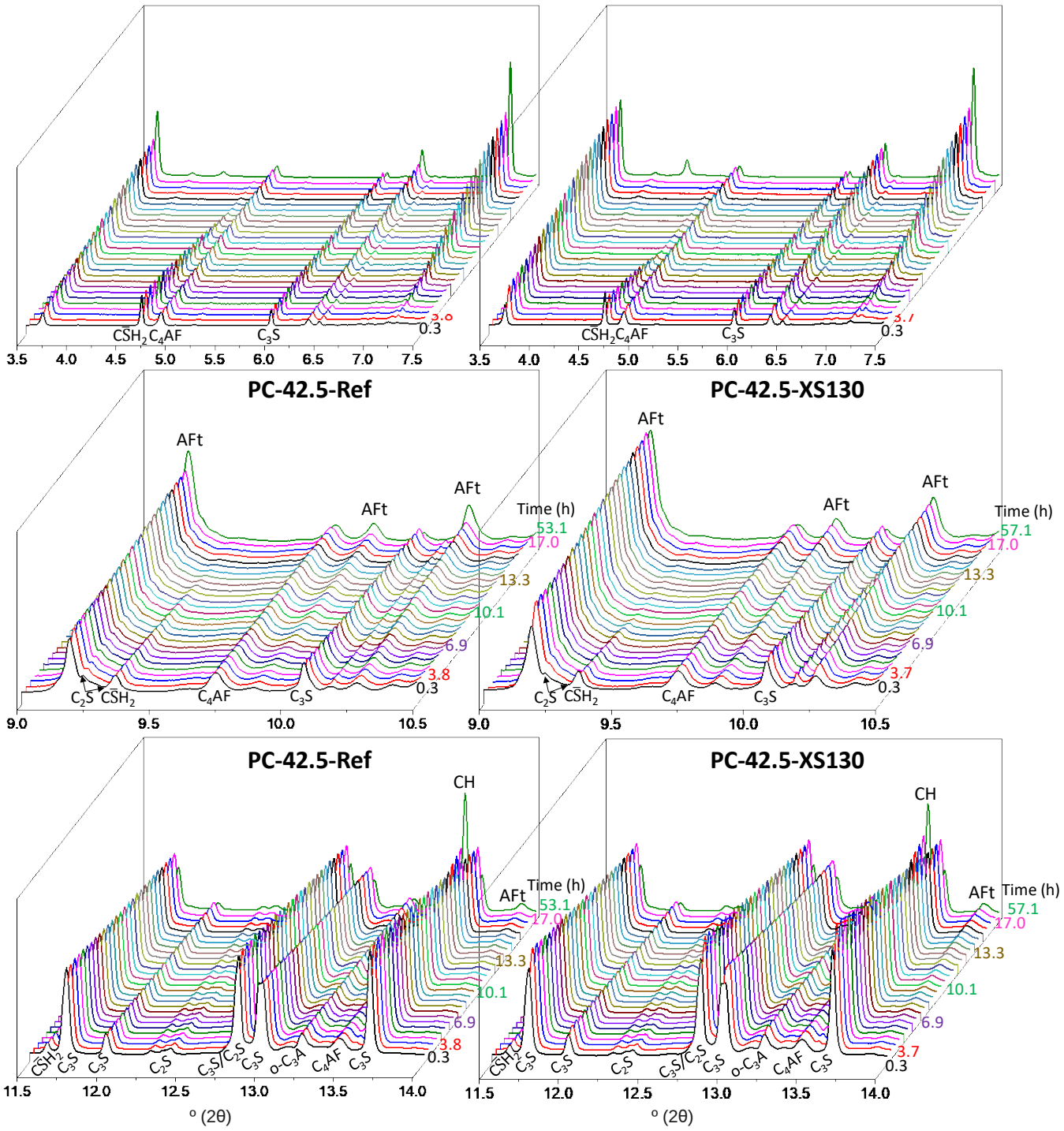

Fig S5. Synchrotron X-ray powder diffraction raw patterns (λ=0.62005 Å) for the PC-42.5-Ref (left panels) and PC-42.5-XS130 (right panels). The 2θ windows have been chosen for better qualitative visualisation of the main phase changes.

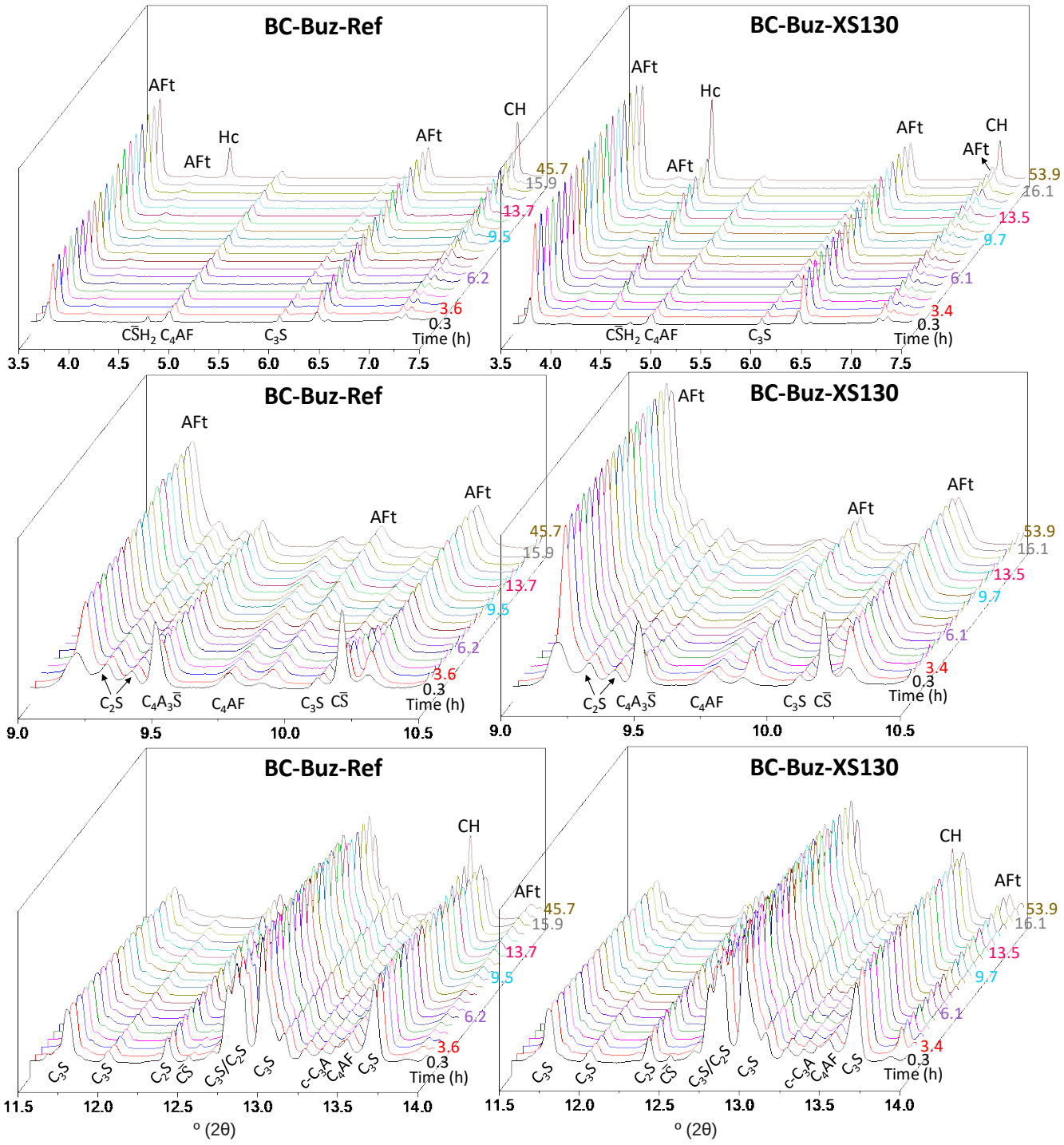

Fig S6. Synchrotron X-ray powder diffraction raw patterns (λ=0.62005 Å) for the BC-Buz-Ref (left panels) and BC-Buz-XS130 (right panels). The 2θ windows have been chosen for better qualitative visualisation of the main phase changes.

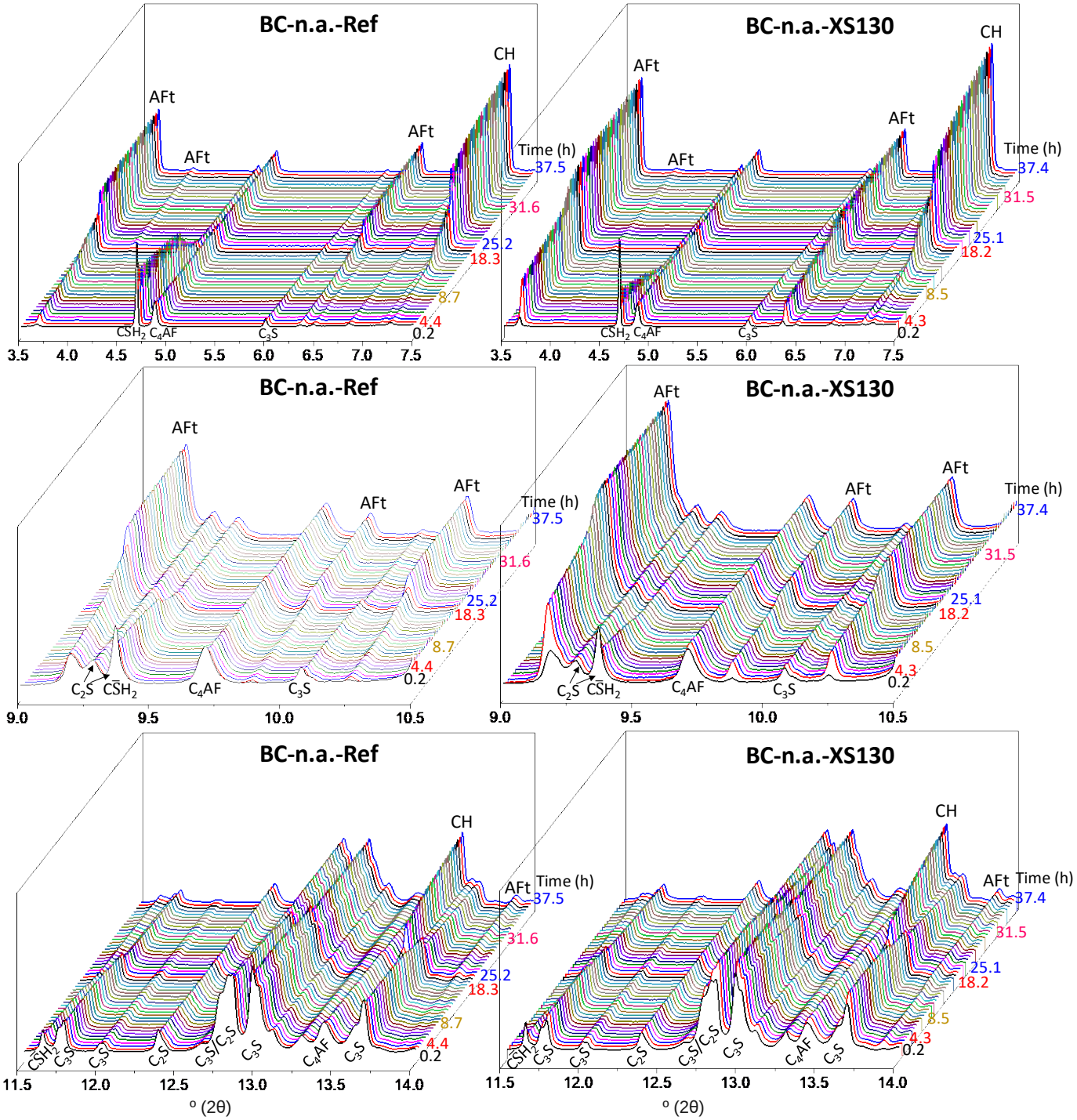

Fig S7. Synchrotron X-ray powder diffraction raw patterns (λ=0.62005 Å) for the BC-n.a.-Ref (left panels) and BC-n.a.-XS130 (right panels). The 2θ windows have been chosen for better qualitative visualisation of the main phase changes.